COMPUTER AND MATHEMATICS WITH APPLICATIONS

EDITOR IN CHIEF: Prof. Leszek Demkowicz, Inst. for Computational Engineering and Sciences (ICES), University of Texas at Austin, Texas, USA.

Accepted September 12th 2016

ISSN : 0898-1221; PUBLISHER- ELSEVIER

5 YEAR IMPACT FACTOR= 1.873

NUMERICAL SOLUTIONS FOR NONLINEAR GYROTACTIC BIOCONVECTION IN NANOFLUID-SATURATED POROUS MEDIA WITH STEFAN BLOWING AND MULTIPLE SLIP EFFECTS

M.J. Uddin
American International University-Bangladesh, Banani, Dhaka 1213, Bangladesh.
Email: jashim_74@yahoo.com
Yasser Alginahi*
Department of Computer Science, Taibah University, P.O. Box 344, Madinah, Saudi Arabia,
Email: yginahi@taibahu.edu.sa
O. Anwar Bég
Fluid Mechanics and Propulsion, Aeronautical and Mechanical Engineering, Room UG17, Newton Building, School of Computing, Science and Engineering (CSE), University of Salford, M54WT, UK. Email: O.A.Beg@salford.ac.uk E-mail gortoab@gmail.com
M.N. Kabir
Faculty of Computer Systems and Software Engineering, University Malaysia Pahang, 26300 Gambang, Pahang, Malaysia, Email: nomanikabir@ump.edu.my

**Corresponding Author-email:* yginahi@taibahu.edu.sa

Abstract:
A mathematical model is developed to examine the effects of the Stefan blowing, second order velocity slip, thermal slip and microorganism species slip on nonlinear bioconvection boundary layer flow of a nanofluid over a horizontal plate embedded in a porous medium with the presence of passively controlled boundary condition. Scaling group transformations are used to find similarity equations of such nanobioconvection flows. The similarity equations are numerically solved with a Chebyshev collocation method. Validation of solutions is conducted with a Nakamura tri-diagonal finite difference algorithm. The effects of nanofluid characteristics and boundary properties such as the slips, Stefan blowing, Brownian motion and Grashof number on the dimensionless fluid velocity, temperature, nanoparticle volume fraction, motile microorganism, skin friction, the rate of heat transfer and the rate of motile microorganism transfer are investigated. The work is relevant to bio-inspired nanofluid-enhanced fuel cells and nano-materials fabrication processes.

Keywords: Second order slip, Porous media; Stefan blowing, Bioconvection, Chebyshev collocation method, Nakamura second order difference scheme, Gyrotactic micro-organisms.

1. INTRODUCTION

Convective flow of fluids containing nanoparticles and micro-organisms is an important area in modern bio-nano-materials processing applications (Das *et al*. 2015). Sakiadis flows, which involve boundary layers on *continuous moving surfaces*, are characteristic of these materials processing operations (Mustafa and Khan 2014). Convective flows over vertical, inclined and horizontal extruding sheets are examples of such flows. Porous media may also

be employed as filtration media to further control such processes (Bég *et al*. 2013). Boundary layer flowsinvolving nano-bioconvection transport can be modelled by the conservation laws of mass, momentum, energy, nano-particle species and micro-organism species. The moving sheet boundary in materials processing operations may also be perforated allowing removal of fluid via *wall suction* or blowing (injection) of fluid via mass flux of certain species from the surface to the ambient medium. Species transfer i.e. *mass diffusion* depends on the flow field and the flow field is also influenced by the mass blowing at the wall. There is therefore strong coupling between momentum and concentration fields. In order to include injection i.e. blowing effects, the Stefan blowing factor, can be introduced as a wall condition to provide a correction in the conservation equations. Models of boundary layer flow are generally solved with no-slip boundary conditions. However, in flows at the nanoscale e.g. hard disk drives, micro-pumps, micro-valves and micro-nozzles, slip phenomena may exhibit at the wall. Especially most non-Newtonian liquids are characterized by slip conditions which in general are governed by a nonlinear relation between the slip velocity and the traction.

Substantial investigations pertaining to bioconvection in nanofluids have been reported in recent years. Kuznetsov (2010) studied the bioconvection in a horizontal layer filled with micro-organisms suspended in a nanofluid using the Buongiorno model. Zaimi *et al*. (2014a) showed that Brownian diffusion and thermophoresis are major factors for producing relative velocity between nanoparticles and the base fluid.The problem was solved using aGalerkin method to obtain the analytical solution for the critical Rayleigh number. The effect of gyrotactic microorganisms is to destabilize compared to nanofluid where the nanoparticles can either reduce or increase the value of the critical Rayleigh number depending on the nanoparticle distribution.Kuznetsov (2011a) explored the onset of nanofluid bio-thermal convection in a horizontal layer of finite depth for the case when the suspension contains gyrotactic and o-xytactic micro-organisms. Kuznetsov (2011b) also investigated oscillatory and non-oscillatory bio-thermal convection of nanofluid in a suspension containing both nanoparticles and gyrotactic microorganisms. Kuznetsov (2011c) further examined nano-bioconvection flow in water-based suspensions considering oscillatory instability. Tham *et al*. (2013a) obtained numerical finite-difference solutions for steady mixed convection from a horizontal circular cylinder embedded in a porous medium saturated by a nanofluid containing both the nanoparticles and gyrotactic microorganisms in a stream flowing vertically upwards. Tham *et al.* (2013b) also studied steady mixed nanofluid convection from a solid sphere. Xu and Pop (2014) explored the effect of nanoparticle volume fraction, distributions of temperature and density of motile microorganisms on fully-developed mixed bioconvection flow in a horizontal channel filled with a nanofluid containing nanoparticles and gyrotactic microorganisms. Zaimi *et. al.*(2014b) used similarity transformations to study the unsteady flow and heat transfer of a nanofluid over a contracting cylinder. Kuznetsov and Nield (2009) extended the Cheng–Minkowycz problem to the case where a porous medium is saturated by a nanofluid. Kuznetsov and Nield (2013) further extended this work (Kuznetsov and Nield, 2009) to the more realistic approach of the boundary being *passively* rather than *actively* controlled. Fang & Jing (2014) investigated flow, heat and mass transfer of a viscous liquid from a stretching sheet by including Stefan blowing effects due to mass transfer under high flux conditions. Their results showed that the blowing effect due to mass transfer can influence velocity profiles, drag, heat flux, and temperature and concentration profiles. Kuznetsov(2011c) proposed a nanofluid formulation in which both nanoparticles and motile (oxytactic) microorganisms are simulated to investigate the stability of the suspension in a shallow horizontal layer. The motility of micro-organisms assists in enhancing mass transfer, microscale mixing, and improves stability of the nanofluid. An analytical solution using the Galerkin method was developed which provided important physical insights into the behavior

of this system; in addition, it was also shown that the oscillatory mode of instability is possible in such system. In another work, Fang (2014) investigated an unsteady stagnation-point flow over a moving wall considering the coupled blowing effect from mass transfer. Rana and Bég (2014) investigated the flow of an incompressible Al2O3–water nanofluid along an inclined permeable plate under transverse magnetic field in a steady 2D mixed convention boundary layer, observing that at a given Richardson number, heat transfer is enhanced with an increase in magnetic field for both pure water and nanofluids, however it is greater in the latter case. Tiwari and Das (2007) conducted a computational investigation on the behavior of nanofluids inside a two-sided lid-driven differentially heated square cavity, showing that the fluid flow and heat transfer in the cavity are affected by Richardson number and the direction of the moving walls. Buongiorno (2006) developed a non-dimensional equilibrium model for mass, momentum and heat transport in nanofluids based on the fact that only Brownian diffusion and thermophoresis are the dominant mechanisms. This study was aimed at explaining the increase in nanofluid heat transfer coefficient above pure fluids, an effect which cannot be predicted by traditional pure fluid correlations. This study also identified that the unusual heat transfer coefficient increase may be attributable to a change in temperature and thermophoresis within the boundary layer. Kothandapani and Prakash (2015) studied the influences of thermal radiation and chemical reactions on peristaltic flow of a Newtonian nanofluid with inclined magnetic field in a vertical channel. They used homotopy perturbation method for their solution and found that the temperature increases as the non-uniform parameter increases whereas it decreases with larger thermal radiation parameter. Uddin *et al.* (2015) studied the two-dimensional magnetohydrodynamic boundary layer flow from a convectively heated permeable vertical surface of an electrically-conducting, chemically-reacting nanofluid. They found that velocity and temperature increases while the nanoparticle volume fraction decreases with the increasing order of chemical reaction. Moreover, as the magnetic field parameter increases the flow is decelerated while the nanoparticle volume fraction and temperature increase. It was also observed that an increase in convection-conduction parameter has no significant influence on nanoparticle volume fraction distribution. Prasad *et al.*(2015) used the Keller box implicit finite difference scheme to explore buoyancy-driven laminar free-convection flow, heat, and mass of a non-Newtonian nanofluid from a horizontal circular cylinder to a micropolar fluid, demonstrating that with greater Brownian motion parameter, temperature, Sherwood number and wall couple stress increase, whereas velocity, concentration, angular velocity, skin friction and Nusselt number decrease. On the other hand, an increase in thermophoresis parameter accelerates the flow and elevates the concentration, angular velocity, skin friction, and Nusselt number, while it decreases the temperature, Sherwood number, and wall couple stress. Yadav *et al.* (2014) investigated magneto-convection in a rotating layer of nanofluid, showing that the critical Rayleigh number is lower for nanofluids compared with regular fluids at the same values of Taylor and Chandrasekhar numbers.

Classical studies in bioconvection were largely mobilized by Platt (1961) who examined bioconvection patterns in cultures of free swimming organism and concluded that the moving polygonal patterns in Tetrahymena, ciliates and flagellates cultures which resemble Benard cells are not due to thermal convection but generated as a result of a dynamic instability due tointernal and mechanical energy input. Much later, Xu (2015) used Lie group analysis to investigate bioconvection flow of a nanofluid in a power law streaming flow. Bég *et al.* (2105) investigated boundary layer bioconvective non-Newtonian nanofluid flow from a horizontal flat plate in a porous medium saturated with microorganisms, noting that bioconvection parameters have significant effects on flow, mass and heat transfer, and motile microorganism density numbers.

Slip effects are also of great relevance in modern engineering designs. Often referred to as non-adherence, slip may be hydrodynamic, thermal or species-related. It may have significant effects on temperature and momentum transport in boundary layer flows. Lawal and Kalyan(1997) developed an analytical solution for the viscous heating in slit and cylindrical tube die flows and proved that the solution can be used to estimate pressure drop and temperature rise in die flows of viscoplastic fluids slip occurring at the wall. Das (2012) studied the nanofluid slip flow and convective heat transfer over a stretching surface, showing that skin friction coefficient decreases with a higher slip parameter and furthermore that slip parameter also lowers the temperature for nanofluids. This study also demonstrated that nanofluids lower the heat transfer rate compared to their own base fluid. Iliuta *et al*. (2002) proposed an updated slip function for the slit models for hydrodynamics of trickle flow reactors. The results showed that the slip function yields liquid holdup and pressure drop with an average absolute error of 17% and 19.5% whereas the error for double slit model is 20% and 18%. Wu (2008) present a slip model for rarefied gas flows at arbitrary Knudsen number. Fang *et al.* (2010) studied viscous flow over a shrinking sheet with a second order slip flow model. Fang and Aziz (2010) discussed viscous flow with second-order slip velocity over a stretching sheet. Uddin *et al.* (2014) investigated the steady 2D magnetohydrodynamic laminar free convective boundary layer slip flow of a nanofluid from a stretching/shrinking sheet in a quiescent fluid, showing that the velocity increases whereas the temperature and concentration decreases with the velocity slip. Uddin *et al.* (2015a) studied the magnetohydrodynamic free convective slip flow of a micropolar fluid over a moving plate. The same authors also investigated the hydromagnetic thermo-solutal nanofluid slip flow in a Darcian porous medium with zero mass flux boundary condition. Beskok and Karniadakis (1994) proposed a mathematical model based on the slip flow theory to simulate heat transport and momentum in complex micro-geometries. Their study investigated the influence of slip flow on skin friction and mass flow rate and the variation of normal stress with Knudsen number.

The aim of the present study is to investigate the collective influence of second order velocity slip, thermal slip, zero mass flux and microorganism slip boundary conditions on the free convection gyrotactic bioconvection boundary layer flow of nanofluid along an upward facing and translating horizontal plate. Lie group analysis is used to derive similarity ordinary differential equations governing the flow. Chebyshev collocation method is employed to solve the resulting well-posed nonlinear boundary value problem. Validation of solutions is achieved with the second order tridiagonal Nakamura difference scheme. The effects of relevant parameters on the dimensionless fluid velocity, temperature, nanoparticle volume fraction, motile microorganism, skin friction, the rate of heat transfer and the rate of motile microorganism transfer are investigated. The present study is relevant to fabrication of nano-bio-materials in industrial manufacturing systems.

2. MATHEMATICAL BIO-NANO-FLUID FORMULATION

The gyrotactic bioconvection boundary layer flow of a Newtonian nanofluid over a horizontal plate located in a porous medium with a moving free stream is considered. The porous medium is assumed to obey Darcy's law and is isotropic and homogenous. Thermal stratification and thermal dispersion effects are neglected. A two-dimensional Cartesian coordinate system $(\bar{x}, \bar{y})$ is used in which the $\bar{x}-$axis is directed along the plate and the $\bar{y}-$axis is aligned in the direction normal to the plate. The flow model with coordinate system is shown in **Fig.1**. It is assumed that the nanofluid contains gyrotactic microorganisms and the flow is steady. It is also assumed that the nanoparticle suspension is stable and the direction of

microorganisms' swimming is independent of nanoparticles. The temperature, nanoparticle volume fraction and density of motile microorganisms are prescribed as T_w , C_w and n_w, respectively at the surface, whereas, T_∞, C_∞ and n_∞ denote their ambient values. Viscous dissipation is neglected in the energy equation. We consider passively controlled boundary conditions as proposed by Kuznetsov and Nield (2014).The following equations describe the conservation of mass, momentum, thermal energy, nanoparticle, and microorganism, respectively, in which the field variables denote the quantities as follows; $\vec{V}$: velocity vector, T : the temperature, C : the nanoparticle volume fraction, and n :the motile microorganism density (Kuznetsov and Nield 2014, Xu and Pop 2014).

$$\nabla \cdot \vec{V} = 0, \tag{1}$$

$$\rho\left(\vec{V}\cdot\nabla\right)\vec{V} = -\nabla p + \mu\nabla^2\vec{V} + (\rho_\infty - \rho)\vec{g} - \frac{\mu}{k_p}\vec{V}, \tag{2}$$

$$\left(\vec{V}\cdot\nabla\right)T = \alpha\,\nabla^2 T + \tau\left[D_B\nabla C\cdot\nabla T + \left(\frac{D_T}{T_\infty}\right)\nabla T\cdot\nabla T\right], \tag{3}$$

$$\left(\vec{V}\cdot\nabla\right)C = D_B\,\nabla^2 C + \left(\frac{D_T}{T_\infty}\right)\nabla^2 T,. \tag{4}$$

$$\vec{V}\cdot\vec{J} = 0. \tag{5}$$

Here $\nabla^2 = \frac{\partial^2}{\partial x^2} + \frac{\partial^2}{\partial y^2}$ and $\vec{V} = (\bar{u},\bar{v})$ is the flow velocity where $(\bar{u},\bar{v})$ are the velocity components along $\bar{x}$ and $\bar{y}$ - axes. According to Kuznetsov (2010), the flux of microorganisms $\vec{J}$ can be expanded in the form as

$$\vec{J} = n\,\vec{V} + n\vec{\bar{V}} - D_n\nabla n, \tag{6}$$

where $\vec{\bar{V}} = \left(\frac{bW_c}{\Delta C}\right)\nabla C,$ in which D_n is the diffusivity of microorganisms, b is the chemotaxis constant [m] and W_c is the maximum cell swimming speed [m/s] (the product bW_c is considered as constant). Using the linear Oberbeck-Boussinesq approximation with the boundary layer approximation, Eqs. (1)-(5) can be written as (Kuznetsov and Nield 2010):

$$\frac{\partial\bar{u}}{\partial\bar{x}} + \frac{\partial\bar{v}}{\partial\bar{y}} = 0, \tag{7}$$

$$\begin{aligned}\rho_f\left(\bar{u}\frac{\partial\bar{u}}{\partial\bar{x}} + \bar{v}\frac{\partial\bar{u}}{\partial\bar{y}}\right) &= \rho_f\,K\,\bar{u}_e\frac{d\bar{u}_e}{d\bar{x}} + \mu\frac{\partial^2\bar{u}}{\partial\bar{y}^2} - \frac{\mu}{k_p\left(\bar{x}/L\right)}\left(\bar{u} - K\,\bar{u}_e\right)\\ &+\left[\left(1-C_\infty\right)\rho_{f_\infty}\beta g\left(T-T_\infty\right) - \left(\rho_p - \rho_{f_\infty}\right)g\left(C-C_\infty\right) + \left(\rho_{m_\infty} - \rho_{f_\infty}\right)g\gamma\left(n-n_\infty\right)\right],\end{aligned} \tag{8}$$

$$\bar{u}\frac{\partial T}{\partial\bar{x}} + \bar{v}\frac{\partial T}{\partial\bar{y}} = \alpha\frac{\partial^2 T}{\partial\bar{y}^2} + \tau\left[D_B\frac{\partial C}{\partial\bar{y}}\frac{\partial T}{\partial\bar{y}} + \left(\frac{D_T}{T_\infty}\right)\left(\frac{\partial T}{\partial\bar{y}}\right)^2\right], \tag{9}$$

$$\bar{u}\frac{\partial C}{\partial\bar{x}} + \bar{v}\frac{\partial C}{\partial\bar{y}} = D_B\frac{\partial^2 C}{\partial\bar{y}^2} + \left(\frac{D_T}{T_\infty}\right)\frac{\partial^2 T}{\partial\bar{y}^2}, \tag{10}$$

$$\bar{u}\frac{\partial n}{\partial \bar{x}}+\bar{v}\frac{\partial n}{\partial \bar{y}}+\frac{\partial}{\partial \bar{y}}\left(n\tilde{v}\right)=D_{n}\frac{\partial^{2} n}{\partial \bar{y}^{2}}.(11)$$

The appropriate boundary conditions can be formulated, following Karniadakis *et al*. (2005) and Fang (2014) as

$$\bar{u}=\bar{u}_{\text{slip}},\ \bar{v}=-\frac{D_B}{\left(1-C_w\right)}\left(\frac{\partial C}{\partial \bar{y}}\right),\ T=T_w+T_{\text{slip}},\ D_B\frac{\partial C}{\partial \bar{y}}+\frac{D_T}{T_\infty}\frac{\partial T}{\partial \bar{y}}=0,$$

$$n=n_w+n_{\text{slip}}\ \text{ at }\ \bar{y}=0, \qquad (12)$$

$$\bar{u}=K\,\bar{u}_e=KU_r\,u_e\left(\bar{x}/L\right),\ T\to T_\infty,\ C\to C_\infty,\ n\to 0\ \text{as}\ \bar{y}\to\infty,$$

where $\tilde{v}=\frac{bW_c}{\Delta C}\frac{\partial C}{\partial \bar{y}}$. α denotes the thermal diffusivity of the fluid, $\tau=\frac{\left(\rho c\right)_{\bar{p}}}{\left(\rho c\right)_f}$ represents the ratio of the effective heat capacity of the nanoparticle to effective heat capacity of the fluid, $\left(\rho c\right)_{\bar{p}}$ is the effective heat capacity of the nanoparticle material, $\left(\rho c\right)_f$ is the effective heat capacity of the fluid, ρ_f is the density of the base fluid, $\rho_{\bar{p}}$ is the density of the nanoparticles, μ is the dynamic viscosity of the base fluid, β is the volumetric expansion coefficient of nanofluid, k is the effective thermal conductivity, K =0 corresponds to an absence of pressure gradient, K=1 corresponds to presence of pressure gradient, g is the gravitational acceleration, D_B stands for the Brownian diffusion coefficient, D_T denotes the thermophoretic diffusion coefficient, D_n is the diffusivity of microorganisms.

$$\bar{u}_{\text{slip}}=\frac{2}{3}\left(\frac{3-\bar{\alpha}\,l^3}{\bar{\alpha}}-\frac{2}{3}\frac{1-l^2}{K_n}\right)\lambda\left(\bar{x}/L\right)\frac{\partial \bar{u}}{\partial \bar{y}}-\frac{1}{4}\left[l^4+\frac{2}{K_n^2}\left(1-l^2\right)\right]\lambda^2\left(\bar{x}/L\right)\frac{\partial^2 \bar{u}}{\partial \bar{y}^2},$$

$$=N_1\left(\bar{x}/L\right)\frac{\partial \bar{u}}{\partial \bar{y}}+N_2\left(\bar{x}/L\right)\frac{\partial^2 \bar{u}}{\partial \bar{y}^2},\ l=\min\left[\frac{1}{K_n},1\right] \qquad (13)$$

where $0\le\bar{\alpha}\le 1$ is the momentum accommodation coefficient and $\lambda\left(\bar{x}/L\right)$ is the molecular mean free path. Based on Knudsen number (K_n), the gas flow in micro channels can be classified into four flow regimes: (i) the continuum flow regime ($K_n\le 0.001$); (ii) slip flow regime ($0.001\le K_n\le 0.1$); (iii) transition flow regime ($0.1\le K_n\le 10$) and (iv) free molecular flow regime ($K_n\ge 10$) (Beskok and Karniadakis 1994). $N_1\left(\frac{\bar{x}}{L}\right)$ is the first order velocity slip factor, $N_2\left(\frac{\bar{x}}{L}\right)$ is the second order velocity slip factor, $T_{\text{slip}}\left(\frac{\bar{x}}{L}\right)=D_1\left(\frac{\bar{x}}{L}\right)\frac{\partial T}{\partial \bar{y}}$ is the thermal slip, $D_1\left(\frac{\bar{x}}{L}\right)$ is the thermal slip factor, $n_{\text{slip}}=E_1\left(\frac{\bar{x}}{L}\right)\frac{\partial n}{\partial \bar{y}}$ is the microorganism slip, $E_1\left(\frac{\bar{x}}{L}\right)$ is the microorganism slip factor, $k_p\left(\bar{x}/L\right)$ is the permeability of the porous medium.

The following non-dimensional variables are introduced to transform Eqns. (7)-(12) into dimensionless form.

$$x=\frac{\bar{x}}{L},\ y=\frac{\bar{y}\sqrt{\text{Re}}}{L},\ u=\frac{\bar{u}}{U_r},\ v=\frac{\bar{v}\sqrt{\text{Re}}}{U_r},\ \theta=\frac{T-T_\infty}{T_w-T_\infty},\ \phi=\frac{C-C_\infty}{C_\infty},\ \chi=\frac{n}{n_w}. \qquad (14)$$

A dimensionless stream function defined by $u = \frac{\partial \psi}{\partial y}$ and $v = -\frac{\partial \psi}{\partial x}$ is introduced into Eqns. (7)-(12), and the following equations emerge:

$$\frac{\partial \psi}{\partial y}\frac{\partial^2 \psi}{\partial x \partial y} - \frac{\partial \psi}{\partial x}\frac{\partial^2 \psi}{\partial y^2} - K u_e \frac{du_e}{dx} - \frac{\partial^3 \psi}{\partial y^3} + \frac{\nu L}{k_p(x) U_r}\left(\frac{\partial \psi}{\partial y} - K u_e\right) - Gr\,\theta + Nr\phi - Rb\,\chi = 0, \quad (15)$$

$$\mathrm{Pr}\left[\frac{\partial \psi}{\partial y}\frac{\partial \theta}{\partial x} - \frac{\partial \psi}{\partial x}\frac{\partial \theta}{\partial y}\right] - \frac{\partial^2 \theta}{\partial y^2} - Nb\,\frac{\partial \theta}{\partial y}\frac{\partial \phi}{\partial y} - Nt\left(\frac{\partial \theta}{\partial y}\right)^2 = 0, \quad (16)$$

$$Sc\left[\frac{\partial \psi}{\partial y}\frac{\partial \phi}{\partial x} - \frac{\partial \psi}{\partial x}\frac{\partial \phi}{\partial y}\right] - \frac{\partial^2 \phi}{\partial y^2} - \frac{Nt}{Nb}\frac{\partial^2 \theta}{\partial y^2} = 0, \quad (17)$$

$$Lb\left[\frac{\partial \psi}{\partial y}\frac{\partial \chi}{\partial x} - \frac{\partial \psi}{\partial x}\frac{\partial \chi}{\partial y}\right] + Pe\,\frac{\partial}{\partial y}\left[\chi\frac{\partial \phi}{\partial y}\right] - \frac{\partial^2 \chi}{\partial y^2} = 0 \quad (18)$$

The boundary conditions in Eqn. (12) become

$$\begin{aligned} &\frac{\partial \psi}{\partial y} = \frac{N_1(x)\mathrm{Re}^{1/2}}{L}\frac{\partial^2 \psi}{\partial y^2} + \frac{N_2(x)\mathrm{Re}}{L^2}\frac{\partial^3 \psi}{\partial y^3},\ \frac{\partial \psi}{\partial x} = \frac{s}{Sc}\frac{\partial \phi}{\partial y},\ \theta = 1 + \frac{D_1(x)\mathrm{Re}^{1/2}}{L}\frac{\partial \theta}{\partial y},\\ &Nt\frac{\partial \phi}{\partial y} + Nb\frac{\partial \theta}{\partial y} = 0,\ \chi = 1 + \frac{E_1(x)\mathrm{Re}^{1/2}}{L}\frac{\partial \chi}{\partial y},\quad \text{at } y = 0,\\ &\frac{\partial \psi}{\partial y} = K u_e(x),\ \theta \to 0,\ \phi \to 0,\quad \chi \to 0,\ \text{as } y \to \infty. \end{aligned} \quad (19)$$

The parameters in Eqns. (15)-(19) are defined as $\mathrm{Pr} = \frac{\nu}{\alpha}$ (Prandtl number), Gr $= \frac{g\beta(T_w - T_\infty)L^3}{\nu^2}$ (thermal Grashof number), $Nt = \frac{\tau D_T (T_w - T_\infty)}{\alpha T_\infty}$ (thermophoresis), $Nb = \frac{\tau D_B (C_w - C_\infty)}{\alpha}$ (Brownian motion), $Nr = \frac{g(\rho_p - \rho_f)C_\infty L}{\rho_f U_r^2}$ (buoyancy ratio), $Le = \frac{\alpha}{D_B}$ (Lewis number), $Rb = \gamma(\rho_p - \rho_{f\infty})n_w L / U_r^2$ (bioconvection Rayleigh number), $Pe = \frac{bW_c}{D_n}$ (Péclet number), $Lb = \nu / D_n$ (bioconvection Lewis number), $Sc = \frac{\nu}{D_B}$ (Schmidt number), $s = \frac{\Delta C}{(1 - C_w)}$ (mass blowing/suction parameter).

3. SIMILARITY TRANSFORMATIONS

To order to obtain the similarity variable, we use the following generalized stretching transformations (Cantwell 2009):

$$x=\alpha_1 x^*,\ y=\alpha_2 y^*,\ \psi=\alpha_3\psi^*,\ \theta=\alpha_4\theta^*,\quad \phi=\alpha_5\phi^*,\chi=\alpha_6\chi^*,$$
$$N_1=\alpha_7 N_1^*, N_2=\alpha_8 N_2^*,\ D_1=\alpha_9 D_1^*, E_1=\alpha_{10} E_2^*,\ k_p=\alpha_{11} k_p^*, u_e=\alpha_9 u_e^*, \tag{20}$$

whereα_i denotes the arbitrary real positive number whose interrelationship is required to be determined for different i = 1,2, …, 12.The boundary layer Eqns. (15) - (18) and boundary conditions in Eqn. (19) will be invariant subject to stretching transformations in Eqn. (20) if the flowing relationship among α_i holds:

$$\alpha_4=\alpha_5=\alpha_6=1, \alpha_2=\alpha_7=\alpha_9=\alpha_{10}=\alpha_1^{1/4}, \alpha_3=\alpha_1^{3/4},\ \alpha_{11}=\alpha_{12}=\alpha_1^{1/2}. \tag{21}$$

Using (21), Eqn. (20) can be simplified as

$$x=\alpha_1 x^*,\ y=\alpha_1^{1/4} y^*,\ \psi=\alpha_1^{3/4}\psi^*,\ \theta=\theta^*,\quad \phi=\phi^*,\chi=\chi^*, N_1=\alpha_1^{1/4} N_1^*,$$
$$D_1=\alpha_1^{1/4} D_1^*, u_e=\alpha_1^{1/2} u_e^*, k_p=\alpha_1^{1/2} k_p^*, N_2=\alpha_1^{1/2} N_2^*, E_1=\alpha_1^{1/4} E_1^*, \tag{22}$$

Eqn. (22) shows that the PDEs along with their boundary conditions would become independent of α_1 for the following combinations of the variables:

$$\frac{y}{x^{\frac{1}{4}}},\ \frac{\psi}{x^{\frac{3}{4}}},\ \theta,\ \phi,\ \chi,\ \frac{u_e}{x^{\frac{1}{2}}},\ \frac{k_p}{x^{\frac{1}{2}}},\ \frac{N_1}{x^{\frac{1}{4}}},\ \frac{N_2}{x^{\frac{1}{2}}},\ \frac{D_1}{x^{\frac{1}{4}}} \text{ and } \frac{E_1}{x^{\frac{1}{4}}}. \tag{23}$$

We define the above functional form as:

$$\eta=\frac{y}{x^{\frac{1}{4}}},\ f(\eta)=\frac{\psi}{x^{\frac{3}{4}}},\ \theta=\theta(\eta),\ \phi=\phi(\eta),\ \chi=\chi(\eta),\ \frac{u_e}{x^{\frac{1}{2}}}=1,$$
$$\frac{k_p}{x^{\frac{1}{2}}}=(k_p)_0, \frac{N_1}{x^{\frac{1}{4}}}=(N_1)_0, \frac{N_2}{x^{\frac{1}{2}}}=(N_2)_0, \frac{D_1}{x^{\frac{1}{4}}}=(D_1)_0, \frac{E_1}{x^{\frac{1}{4}}}=(E_1)_0, \tag{24}$$

where$(N_1)_0, (N_2)_0, (D_1)_0, (E_1)_0, (k_p)_0$ are constants of the first order momentum slip factor, second order momentum slip factor, thermal slip factor, microorganism slip factor and permeability. Here $f(\eta)$, $\theta(\eta)$, $\phi(\eta)$ and $\chi(\eta)$ are respectively the dimensionless velocity, temperature, nanoparticle volume fraction and density of motile microorganism and η is the similarity independent variable.

3.2 SIMILARITY DIFFERENTIAL EQUATIONS

By substituting the transformations in Eqn. (24) into Eqns. (15)- (19), we find the following similarity equations:

$$f'''+\frac{3}{4} f f''+\frac{1}{2}\left(K-f'^2\right)-\frac{1}{Da}\left(f'-K\right)+Gr\,\theta-Nr\,\phi+Rb\,\chi=0, \tag{25}$$

$$\theta''+\frac{3}{4}\Pr f\,\theta'+Nb\,\theta'\phi'+Nt\,\theta'^2=0 \tag{26}$$

$$\phi''+\frac{3}{4}Sc\,f\phi'+\frac{Nt}{Nb}\theta''=0, \tag{27}$$

$$\chi''+\frac{3}{4}Lb\,f\chi'-Pe\left(\phi''\chi+\phi'\chi'\right)=0. \tag{28}$$

Then the boundary conditions reduce to:

$$f(0)=\frac{4s\phi'(0)}{3Sc},\ f'(0)=a\,f''(0)+b\,f'''(0),\theta(0)=1+c\,\theta'(0),\ Nb\,\phi'(0)+Nt\,\theta'(0)=0,$$
$$\chi(0)=1+d\,\chi'(0),\ f'(\infty)=K,\ \theta(\infty)=0,\ \phi(\infty)=0,\ \chi(\infty)=0, \tag{29}$$

where the prime denotes differentiation with respect to η. Dimensionless slip parameters are defined as $a=\frac{(N_1)_0\,\mathrm{Re}^{1/2}}{L}>0$ (first order velocity slip), $b=\frac{(N_2)_0\,\mathrm{Re}}{L^2}<0$ (second order velocity slip), $c=\frac{(D_1)_0\,\mathrm{Re}^{1/2}}{L}$ (thermal slip) and $d=\frac{(F_1)_0\,\mathrm{Re}^{1/2}}{L}$ (microorganism slip).

It is noticed that in the absence of pressure gradient (K=0) and in the absence of microorganism equation, our model reduces to that previously considered by Uddin *et al.* (2014). To check the validity of our model we have compared our results with Uddin *et al.* (2014) and comparison is given in **Table 1.** Very good agreement is achieved. Confidence in the present computations is therefore justifiably high.

4. PHYSICAL QUANTITIES

Parameters of engineering interest are the local skin friction factor $C_{f\bar{x}}$, the local Nusselt number $Nu_{\bar{x}}$, the local density number of the motile microorganisms $Nn_{\bar{x}}$. Physically, $C_{f\bar{x}}$ indicates wall shear stress, $Nu_{\bar{x}}$ denotes the rate of heat transfer and $Nn_{\bar{x}}$ represents the rate of micro-organism transfer. They are computed using the following relations:

$$C_{f\bar{x}}=\frac{2\mu}{\rho\bar{u}_e^2}\left(\frac{\partial\bar{u}}{\partial\bar{y}}\right)_{\bar{y}=0},\quad Nu_{\bar{x}}=\frac{-\bar{x}}{T_w-T_\infty}\left(\frac{\partial T}{\partial\bar{y}}\right)_{\bar{y}=0},$$
$$Sh_{\bar{x}}=\frac{-\bar{x}}{C_w-C_\infty}\left(\frac{\partial C}{\partial\bar{y}}\right)_{\bar{y}=0},\ Nn_{\bar{x}}=\frac{-\bar{x}}{n_w-n_\infty}\left(\frac{\partial n}{\partial\bar{y}}\right)_{\bar{y}=0}. \tag{30}$$

By substituting from Eqns. (14) and (24) into Eqn. (30), we obtain that

$$\mathrm{Re}_{\bar{x}}^{1/2}\,C_{f\bar{x}}=f''(0),\ \mathrm{Re}_{\bar{x}}^{-1/2}\,Nu_{\bar{x}}=-\theta'(0),$$
$$\mathrm{Re}_{\bar{x}}^{-1/2}\,Sh_{\bar{x}}=-\frac{\phi'(0)}{\phi(0)},\ \mathrm{Re}_{\bar{x}}^{-1/2}\,Nn_{\bar{x}}=-\chi'(0) \tag{31}$$

Here $\mathrm{Re}_{\bar{x}}=\bar{u}_e\,\bar{x}/\nu$ is the local Reynolds number.

5. CHEBYCHEV COLLOCATION COMPUTATIONAL SOLUTION

The transformation of the original governing equations into a form of ODEs reduces the boundary value problem complexity significantly and facilitates a numerical solution.We aim to solve Eqns. (25)–(28) with the boundary conditions (29) using the Chebyshev collocation method. Hence, the equations which are of higher order are transformed into second order ODEs. Suppose that$F_1=f,\ F_2=f',\ F_3=\theta,\ F_4=\phi,\ F_5=\chi$.Using the new variables in Eqns. (25)–(28), the boundary value problem can be formulated as the following system of ODEs:

$$\underbrace{\begin{bmatrix} F_1'' \\ F_2'' \\ F_3'' \\ F_4'' \\ F_5'' \end{bmatrix}}_{F''} = \underbrace{\begin{bmatrix} F_2' \\ 1/Da(F_2-1) - Gr\,F_3 + Nr\,F_4 - Rb\,F_5 - 0.75F_1DF_2 - 0.5(1-F_2^2) \\ -0.75\,\mathrm{Pr}\,F_1F_3' - Nb\,F_3'F_4' - Nt\,F_3'^2 \\ \frac{Nt}{Nb}(0.75\,\mathrm{Pr}\,F_1F_3' + Nb\,F_3'F_4' + Nt\,F_3'^2) - 0.75\,Sc\,F_1'F_4' \\ PeF_5\left[\frac{Nt}{Nb}(0.75\,\mathrm{Pr}\,F_1F_3' + Nb\,F_3'F_4' + Nt\,F_3'^2) - 0.75\,Sc\,F_1'F_4'\right] + PeF_4'F_5' - 0.75\,Lb\,F_1'F_5' \end{bmatrix}}_{g(\eta,F,F')} \quad (32)$$

which implies that F'' is a function of η, $F := [F_1, F_2, F_3, F_4, F_5]^T$ and F'. Note that Eq. (32) contains a vector of five variables with five equations in. We now discuss how boundary conditions (29) are transformed using the new set of variables. Note that the velocity slip boundary condition in (29) contains a third derivative term which poses another difficulty to solve Eq. (32). Therefore the velocity slip boundary condition is converted using Eq. (25) as follows:

$$f'(0) = 1 + af''(0) + bf'''(0) \quad (33a)$$

From the above equation, we deduce that

$$f'''(0) = \frac{f'(0)-1-af''(0)}{b} \quad (33b)$$

Finally, the boundary conditions for the variables using Eqns. (29) and (33) can be formulated as follows:

$$\left.\begin{aligned} F_1(0) &= \frac{4s}{3Sc}F_4(0) \\ F_2''(0) &= \frac{F_2(0)-1-a\ F_2'(0)}{b} \\ F_3(0) &= 1 + cF_3'(0) \\ F_4'(0) &= -\frac{Nt\,F_3'(0)}{Nb} \\ F_5(0) &= 1 + dF_5'(0) \\ F_1'(\infty) &= F_2(\infty) = 1 \\ F_3(\infty) &= 0 \\ F_4(\infty) &= 0 \\ F_5(\infty) &= 0 \end{aligned}\right\} \quad (34)$$

First, nonlinear ODEs are discretized at n-Chebyshev collocation points x_j between [-1, 1] which is the Chebyshev domain with $x_j = \cos(j\pi/n)$. The derivative of F is approximated by Chebyshev derivative DF where D is an $(n+1) \times (n+1)$ matrix with

$$\left.\begin{aligned} D_{00} &= \frac{2n^2+1}{6} \\ D_{nn} &= -\frac{2n^2+1}{6} \\ D_{jj} &= \frac{-x_j}{2(1-x_j^2)} \quad \text{for } j = 1, \dots, n-1 \\ D_{ij} &= \left(\frac{c_i}{c_j}\right)\frac{(-1)^{i+j}}{(x_i-x_j)} \quad \text{for i} \neq j, i, j = 1, \dots, n-1 \end{aligned}\right\} \quad (35)$$

where $c_i = \begin{cases} 2 & i = 0 \text{ or } N \\ 1 & \text{otherwise} \end{cases}$.

The second derivative can be calculated using D^2F where $D^2 = D \times D$. Finally eqn (32) provides a system of $5 \times (n+1)$ nonlinear equations. The actual range of physical domain η is $[0, \infty]$. However, it is observed that $\eta = 10$ is sufficient to represent the upper bound $\eta = \infty$.

Therefore, the Chebyshev collocation domain [-1 1] are required to be mapped on the physical domain [0, 10] where the mapping can be trivially found as

$$x = \frac{\eta - 5}{5} \tag{36}$$

In the Chebyshev domain, the system of equations (32) will take the form:

$$\underbrace{\begin{bmatrix} D^2F_1 \\ D^2F_2 \\ D^2F_3 \\ D^2F_4 \\ D^2F_5 \end{bmatrix}}_{F''} = \underbrace{\begin{bmatrix} 5DF_2 \\ 251/Da(F_2 - 1) - 25Gr\,F_3 + 25Nr\,F_4 - 25Rb\,F_5 - 3.75F_1DF_2 - 12.5(1 - F_2^2) \\ -3.75\,\mathrm{Pr}\,F_1DF_3 \; - 5NbDF_3DF_4 - 5Nt\,DF_3 \\ \frac{Nt}{Nb}(3.75\,\mathrm{Pr}\,F_1DF_3 + Nb\,DF_3DF_4 + NtDF_3^2) - 0.75\,Sc\,DF_1DF_4 \\ PeF_5\left[\frac{Nt}{Nb}(3.75\,\mathrm{Pr}\,F_1DF_3 + Nb\,DF_3DF_4 + NtDF_3^2) - 0.75\,Sc\,DF_1DF_4\right] + PeDF_4DF_5 - 0.75\,Lb\,DF_1DF_5 \end{bmatrix}}_{g(x,F,F')} \tag{37}$$

with the boundary conditions

$$\left.\begin{aligned} F_1(0) &= \frac{4s}{3Sc}F_4(0) \\ D^2F_2(0) &= \frac{F_2(0) - 1 - aDF_2(0)}{b} \\ DF_3(0) &= \frac{F_3(0) - 1}{0.2\,c} \\ DF_4(0) &= -\frac{Nt}{Nb}\left(\frac{F_3(0) - 1}{0.2c}\right) \\ DF_5(0) &= \frac{F_5(0) - 1}{0.2d} \\ DF_1(n) &= F_2(n) = 5 \\ F_3(n) &= 0 \\ F_4(n) &= 0 \\ F_5(n) &= 0 \end{aligned}\right\} \tag{38}$$

Now expanding D^2F_1it may be shown that:

$$D^2F_1 = \begin{bmatrix} D_{00}^2 & D_{01}^2 & \cdots & D_{0n}^2 \\ D_{10}^2 & D_{11}^2 & \cdots & D_{1n}^2 \\ \vdots & \vdots & \vdots & \vdots \\ D_{n0}^2 & D_{n1}^2 & \cdots & D_{nn}^2 \end{bmatrix}\begin{bmatrix} F_{1,0} \\ F_{1,1} \\ \vdots \\ F_{1,n} \end{bmatrix} = \begin{bmatrix} 5F_{2,0} \\ 5F_{2,1} \\ \vdots \\ 5F_{2,n} \end{bmatrix} \tag{39}$$

Finally the boundary conditions are required to be set in the equations. The boundary conditions are set in the appropriate (boundary) positions by replacing the corresponding discretized equations. For the Eqn. of D^2F_1, we replace the first and $(n+1)$-th equations by the corresponding boundary equations provided in (34).

$$D^2F_1 = \begin{bmatrix} 1 & 0 & \cdots & 0 \\ D_{10}^2 & D_{11}^2 & \cdots & D_{1n}^2 \\ \vdots & \vdots & \vdots & \vdots \\ D_{(n-1)0}^2 & D_{(n-1)1}^2 & \cdots & D_{(n-1)n}^2 \\ D_{n0} & D_{n0} & \cdots & D_{n0} \end{bmatrix}\begin{bmatrix} F_{1,0} \\ F_{1,1} \\ \vdots \\ F_{1,n-1} \\ F_{1,n} \end{bmatrix} = \begin{bmatrix} \frac{4s}{3Sc}F_4(0) \\ 5F_{2,1} \\ \vdots \\ 5F_{2,n-1} \\ 5 \end{bmatrix} \tag{40}$$

Thus all other boundary conditions are set for DF_2, DF_3, …,DF_5. The resulting system is a large nonlinear system of equations of $5\times n$unknowns with $5\times n$ equations which can be solved using aNewton-type iterative method. The system of equations generated has been solved using the MATLAB trust-region-reflective algorithm *fsolve*. Finally the solution is mapped to the physical domain using the transformation:

$$\eta = 5x + 5 \tag{41}$$

6. VALIDATION WITH NAKAMURA DIFFERENCE SCHEME

To verify the accuracy of our Chebychev collocation method (CCM) solutions, we employ an alternative method to solve the present boundary value problem. This alternate algorithm,

specifically the Nakamura tridiagonal method (Nakamura 1994) was introduced originally to solve rheological (e.g. micropolar) heat transfer problems. Hereafter referred to as **NTM**, in this approach the 9th order system of nonlinear, multi-degree, coupled ordinary differential equations (25)–(28) with boundary conditions (29) is solved using NANONAK code (Bég 2013), in double precision arithmetic in Fortran 90. Computations are performed on an SGI Octane Desk workstation with dual processors and take seconds for compilation. A reduction in the higher order differential equations is fundamental principle to **NTM** like other difference methods. Furthermore, it is particularly effective for simulating complex fluid (rheological) boundary layer flows due to their parabolic nature. **NTM** has been successfully deployed in swirling micropolar convection (Gorla and Nakamura 1993), viscoelastic Falkner-Skan flows (Bég*et al.* 2004) and quite recently in magnetohydrodynamic external boundary layer flows of micropolar biopolymers ((Bég *et al.* 2014). **NTM** is equally adept at solving both one-dimensional (ordinary differential system) and two-dimensional (partial differential system) *non-similar non-Newtonian* flows. Intrinsic to this method is the discretization of the boundary layer regime using an equi-spaced finite difference mesh in the transformed coordinate (η). The partial derivatives for f, g, θ with respect to η are evaluated by central difference approximations. An iteration loop based on the method of successive substitution is utilized to advance the solution. The finite difference discretized equations are solved in a step-by-step fashion on the ηdomain. For the energy, nano-particle species and motile micro-organism density conservation Eqns. (26) - (28) which are *second order* multi-degree ordinary differential equations, only a *direct substitution* is needed. However a reduction is required for the *third order* momentum Eqn. (25). We apply the following substitutions:

$$P = f' \tag{42}$$

$$Q = \theta \tag{43}$$

$$R = \phi \tag{44}$$

$$S = \chi \tag{45}$$

The ODEs (25)-(28) then retract to:

Nakamura momentum equation:

$$A_1 P'' + B_1 P' + C_1 P = T_1 \tag{46}$$

Nakamura energy equation:

$$A_2 Q'' + B_2 Q' + C_2 Q = T_2 \tag{47}$$

Nakamura nano-particle species equation:

$$A_3 R'' + B_3 R' + C_3 R = T_3 \tag{48}$$

Nakamura motile micro-organism density number equation:

$$A_4 S'' + B_4 S' + C_4 S = T_4 \tag{49}$$

Here A_i*=1,2,3,4,* B_i*=1,2,3,4,* C_i*=1,2,3,4*are the coefficients of Nakamura matrix, T_i*=1,2,3,4* are the Nakamura source terms comprising the parameters, variables (P, Q, R, S) and their derivatives. The Nakamura Eqns. (46)–(49) are transformed to finite difference equations and these are orchestrated to form a tridiagonal system which is iteratively solved due to the high nonlinearity of the numerous coupled and multi-degree terms in the momentum, energy,

nano-particle species and motile micro-organism density conservation equations. The boundary conditions (29) are also easily transformed. Further details of the **NTM** approach are provided in the comprehensive treatise of Nakamura (1995). More recent and sophisticated applications covering many different non-Newtonian flows (with magnetic effects) are also reviewed by Bég (2012). **Tables1-4** provide both CCM MATLAB and NTM solutions for shear stress function, *f''(0),* dimensionless wall heat transfer rate, *-θ'(0),* dimensionless wall nano-particle mass transfer rate function, *-ϕ'(0)/ϕ(0)* and dimensionless motile micro-organisms wall mass transfer rate, *-χ'(0)* for a variation in six key thermophysical parameters, namely $s = \frac{\Delta C}{(1-C_w)}$ (mass blowing/suction parameter), $a = \frac{(N_1)_0 \,\mathrm{Re}^{1/2}}{L} > 0$ (first order velocity slip), $b = \frac{(N_2)_0 \,\mathrm{Re}}{L^2} < 0$ (second order velocity slip), $c = \frac{(D_1)_0 \,\mathrm{Re}^{1/2}}{L}$ (thermal slip), $d = \frac{(F_1)_0 \,\mathrm{Re}^{1/2}}{L}$ (microorganism slip) and $Gr = \frac{g\beta(T_w - T_\infty)L^3}{\nu^2}$ (thermal Grashof number). All other model parameters are prescribed as *Lb=Pe=Rb=Sc=2*, *Da* = 0.5, *Nb* = *Nr* =*Nt* = 0.1 in **Tables 1-4**.The agreement is very close in all the tables testifying to the accuracy of the CCM MATLAB solutions. Confidence in **CCM** computations is therefore very high. In **Table 1**, we observe that with positive *s* values (suction) the shear stress values generally decrease whereas they strongly increase with negative *s* values (mass blowing at the wall).Increasing first order hydrodynamic slip (*a*) is found to generally reduce shear stress magnitudes i.e. decelerate the boundary layer flow. Increasingly negative values of second order hydrodynamic slip (*b*) with all other parameters fixed, induce an even greater deceleration in the flow i.e. they more prominently reduce the shear stress (*f''(0)*) values. A strong increase in thermal slip (*c*) results in a much weaker deceleration in the flow for blowing (*s*<0) and a solid wall (*s* =0) whereas the converse effect i.e. weak acceleration is induced with suction at the wall (*s*>0). Increasing micro-organism slip is observed in **Table 1** to again decelerate the flow, however in this case this is only apparent for suction or blowing. With a solid wall (*s*=0) greater micro-organism slip weakly enhances skin friction i.e. shear stress magnitudes. With decrease in thermal Grashof number (*Gr* =-4) shear stress values are generally enhanced whereas with increase i.e. for *Gr* =4, they strongly decrease. This indicates that an assistive buoyancy force (*Gr*>0 and *Grθ*>0 in the momentum eqn.(25)) decelerates the boundary layer flow whereas an opposing buoyancy force accelerates the flow, a characteristic which has been reported in many studies and is documented in detail by Gebhart*et al.* (1988).

Table 1: Values of *f''(0)*when *Lb=Pe=Rb=Sc=2*, *Da* = 0.5, *Nb* = *Nr* = *Nt* = 0.1.

s	*a*	*b*	*c*	*d*	*Gr*	*f''(0)[CCM MATLAB]*	*f''(0) [NTM]*
-1						0.8498531	0.84990
0	0.1	-0.5	0.5	0.5	1	0.7385858	0.73860
1						0.272482	0.27248
-1						0.1036811	0.10369
0	10	-0.5	0.5	0.5	1	0.0901492	0.090150
1						0.037396	0.037401
-1						1.4479129	1.447912
0	0.5	0	0.5	0.5	1	1.5642195	1.564220
1						1.5562531	1.556254
-1						-0.2275983	-0.227598

0 1	0.5	-5	0.5	0.5	1	-0.4027906 -0.6767009	-0.402791 -0.676701
-1 0 1	0.5	-0.5	0.1	0.5	1	0.6581322 0.5716338 0.2171846	0.6581320 0.5716331 0.2171843
-1 0 1	0.5	-0.5	2	0.5	1	0.5652345 0.5080153 0.4503765	0.5652342 0.5080151 0.4503763
-1 0 1	0.5	-0.5	0.5	0	1	0.679755 0.5677279 0.2995202	0.6797548 0.5677277 0.2995201
-1 0 1	0.5	-0.5	0.5	1	1	0.6417392 0.5730997 0.0631091	0.6417391 0.5730996 0.0631090
-1 0 1	0.5	-0.5	0.5	0.5	-4	0.7588097 0.9000447 0.4509315	0.7588096 0.9000444 0.4509312
-1 0 1	0.5	-0.5	0.5	0.5	4	0.4950872 0.3688626 0.0790472	0.4950871 0.3688624 0.0790471

Table 2: Values of -θ'(0), when *Lb=Pe=Rb=Sc=2*, *Da* = 0.5, *Nb* = *Nr* = *Nt* = 0.1.

s	*a*	*b*	*c*	*d*	*Gr*	*-θ'(0) [CCM MATLAB]*	*-θ'(0)[NTM]*
-1 0 1	0.1	-0.5	0.5	0.5	1	0.607438 1.008712 1.503294	0.607439 1.008711 1.503290
-1 0 1	10	-0.5	0.5	0.5	1	0.657162 1.046634 1.506314	0.657161 1.046631 1.506312
-1 0 1	0.5	0	0.5	0.5	1	0.561513 0.949240 1.484832	0.561511 0.949242 1.484833
-1 0 1	0.5	-5	0.5	0.5	1	0.677280 1.071530 1.514872	0.677281 1.071531 1.514874
-1 0 1	0.5	-0.5	0.1	0.5	1	0.620913 1.019095 1.504013	0.620916 1.019097 1.504013
-1 0 1	0.5	-0.5	2	0.5	1	0.356276 0.396366 0.426287	0.356278 0.396362 0.426282
-1 0 1	0.5	-0.5	0.5	0	1	0.634018 1.007277 1.497892	0.634014 1.007274 1.497893
-1 0 1	0.5	-0.5	0.5	1	1	0.611347 1.034068 1.513349	0.611341 1.034067 1.513347
-1 0	0.5	-0.5	0.5	0.5	-4	0.471824 0.942547	0.471823 0.942545

1						1.498561	1.498562
-1 0 1	0.5	-0.5	0.5	0.5	4	0.672204 1.049958 1.507061	0.672202 1.049956 1.507059

Table 3: Values of $-\phi'(0)/\phi(0)$, when $Lb=Pe=Rb=Sc=2$, $Da = 0.5$, $Nb = Nr = Nt = 0.1$.

s	*a*	*b*	*c*	*D*	*Gr*	*-φ′(0)/φ(0) [CCM MATLAB]*	*-φ′(0)/φ(0) [NTM]*
-1 0 1	0.1	-0.5	0.5	0.5	1	0.953982 3.143614 22.743586	0.953983 3.143612 22.74359
-1 0 1	10	-0.5	0.5	0.5	1	1.093983 3.461709 22.762038	1.093984 3.461706 22.762037
-1 0 1	0.5	0	0.5	0.5	1	0.835513 2.695851 22.621909	0.835512 2.695849 22.62191
-1 0 1	0.5	-5	0.5	0.5	1	1.154128 3.684549 22.806773	1.154127 3.684548 22.806774
-1 0 1	0.5	-0.5	0.1	0.5	1	0.990660 3.228023 22.746791	0.990663 3.228024 22.746788
-1 0 1	0.5	-0.5	2	0.5	1	1.550431 2.944010 5.827033	1.550433 2.944013 5.827034
-1 0 1	0.5	-0.5	0.5	0	1	1.024188 3.143874 22.970731	1.024187 3.143876 22.970733
-1 0 1	0.5	-0.5	0.5	1	1	0.966659 3.337841 22.473316	0.966657 3.337843 22.473318
-1 0 1	0.5	-0.5	0.5	0.5	-4	0.638963 2.667635 22.767563	0.638965 2.667636 22.767564
-1 0 1	0.5	-0.5	0.5	0.5	4	1.134764 3.481403 22.741677	1.134762 3.481405 22.741678

Table 4: Values of $-\chi'(0)$ when $Lb=Pe=Rb=Sc=2$, $Da = 0.5$, $Nb = Nr = Nt = 0.1$.

s	*a*	*b*	*c*	*D*	*Gr*	*-χ′(0) [CCM MATLAB]*	*-χ′(0) [NTM]*
-1		-0.5	0.5	0.5	1	0.353847	0.353845

0 1	0.1					-0.341015 -0.916316	-0.341014 -0.916314
-1 0 1	10	-0.5	0.5	0.5	1	0.338232 -0.358415 -0.877928	0.338234 -0.358416 -0.877930
-1 0 1	0.5	0	0.5	0.5	1	0.369275 -0.296581 -1.158394	0.369272 -0.296585 -1.158393
-1 0 1	0.5	-5	0.5	0.5	1	0.332735 -0.363668 -0.768862	0.332737 -0.363664 -0.768863
-1 0 1	0.5	-0.5	0.1	0.5	1	0.349562 -0.346816 -0.907642	0.349559 -0.346812 -0.907644
-1 0 1	0.5	-0.5	2	0.5	1	0.364792 0.374168 0.454835	0.364790 0.374164 0.454832
-1 0 1	0.5	-0.5	0.5	0	1	0.427789 -0.298392 -0.668139	0.427784 -0.298397 -0.668131
-1 0 1	0.5	-0.5	0.5	1	1	0.296029 -0.410949 -1.242199	0.296022 -0.410941 -1.242190
-1 0 1	0.5	-0.5	0.5	0.5	-4	0.369968 -0.310925 -0.980525	0.369959 -0.310930 -0.980529
-1 0 1	0.5	-0.5	0.5	0.5	4	0.343265 -0.351406 -0.866608	0.343266 -0.351410 -0.866611

Table 2 indicates that with blowing at the wall, heat transfer rates are lower than with suction at the wall. With greater first order (a) and second order slip (b), however heat transfer rates are generally enhanced irrespective of whether blowing or suction is present at the wall. With increasing thermal slip (c) there is generally a strong reduction in wall heat transfer rate. With increasing micro-organism slip (d) the heat transfer rate decreases for blowing at the wall whereas it is elevated weakly with greater suction or for the case of a solid wall. With negative thermal Grashof number, the heat transfer rate decreases whereas with positive Grashof number it increases, in particular for the case of wall blowing (mass injection) i.e. $s<0$). **Table 3** shows that nano-particle mass transfer function is massively greater for the case of suction and lowest for blowing, implying that reduction in fluid momentum encourages nano-particle diffusion at the wall. With greater first order (a) and second order hydrodynamic slip (b), $-\varphi'(0)/\varphi(0)$ function values strongly increase. With increasing thermal slip (c), nano-particle mass transfer function increases for the case of blowing at the wall; however $-\varphi'(0)/\varphi(0)$ function values significantly fall for the solid wall case ($a=0$) or with suction at the wall ($a>0$). With increasing micro-organism slip (d), nano-particle mass transfer function, $-\varphi'(0)/\varphi(0)$ rises for the solid wall case ($s=0$) but drops when blowing ($s<0$) or suction ($s>0$) are present. With increasing Grashof number, i.e. when Gr = 4 compared to when it is -4, the nano-particle mass transfer function, $-\varphi'(0)/\varphi(0)$strongly increases for the blowing or solid wall case but slightly reduces when wall suction is present. **Table 4**

demonstrates that with increasing first order hydrodynamic slip (a), motile micro-organism density transfer rate decreases for both the case of a solid wall or wall blowing, but increases for the wall suction scenario. Similarly with increasing second order hydrodynamic slip (*b*), *-χ′(0) again* falls for both wall blowing and the solid wall, but rises for the wall suction case. With greater thermal slip (c), the motile micro-organism density transfer rate, *-χ′(0), is consistently enhanced for all three wall cases i.e. for blowing, solid wall or suction cases. Conversely, w*ith rising micro-organism slip (*d*) *-χ′(0) consistently drops for all three cases of blowing, solid wall or wall suction.* Finally an elevation in Grashof number (*Gr*) from negative to positive values, induces strong decrease in the motile micro-organism density transfer rate, *-χ′(0),* for both the wall injection (blowing) and solid wall cases but results in a slight elevation for the wall suction case. As elaborated earlier, very close agreement for all computations for all the values of the thermophysical and bioconvection parameters is achieved between CCM MATLAB and NTM approaches.

7. CHEBYCHEV COLLOCATION RESULTS AND DISCUSSION

In order to establish the influence of the emerging bioconvection and thermal parameters on the flow variables i.e. dimensionless velocity $f'(\eta)$, temperature $\theta(\eta)$, the nanoparticle volume fraction $\phi(\eta)$ and the microorganism concentration $\chi(\eta)$, with zero mass flux boundary conditions, extensive computations have been conducted with the MATLAB CCM approach. In the simulation, we consider a water based nanofluid with the following prescribed values: *Pr* = 6.8 (water), *Rb*= 1, *Nr = Nt = 0.1*. Unless otherwise stated, the following default values are imposed in the computations: *a = 0.1, b = -0.5, c = 0.5, d = 0.5, Gr = 1, Lb = 2, M = 2, Nb = Nr = Nt = 0.1, Pe = 2, Rb = 2, Sc = 2.* **Figs. 2-13**are provided to illustrate the results. In all these figures, field quantities *must approach asymptotically towards zero in the free stream*i.e., $f'(\eta) \to 0$, $\theta(\eta) \to 0$, $\phi(\eta) \to 0$ and $\chi(\eta) \to 0$ as $\eta \to \infty$. This is satisfied by $f'(\eta)$, $\phi(\eta)$, $\theta(\eta)$ and $\chi(\eta)$ which clearly tend to zero as $\eta \to 20$ (i.e., the infinity boundary condition imposed for η is sufficiently large) as observed in all the figures. This confirms that the correct numerical solutions are obtained. Our solutions $f'(\eta)$, $\phi(\eta)$, $\theta(\eta)$ and $\chi(\eta)$ at $\eta = 20$ have the accuracy of the order of $O(10^{-10})$.The NTM solutions discussed earlier have an accuracy of $O(10^{-8})$ which is more than sufficient for low-speed, heat and mass transfer in boundary layer flows.

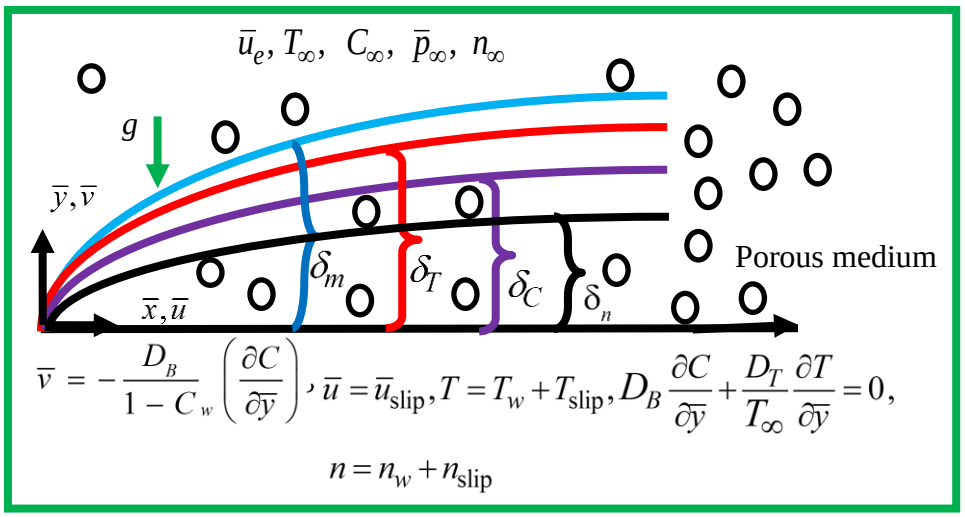

Fig. 1: Coordinate system and nanofluid bioconvection wall slip flow model.

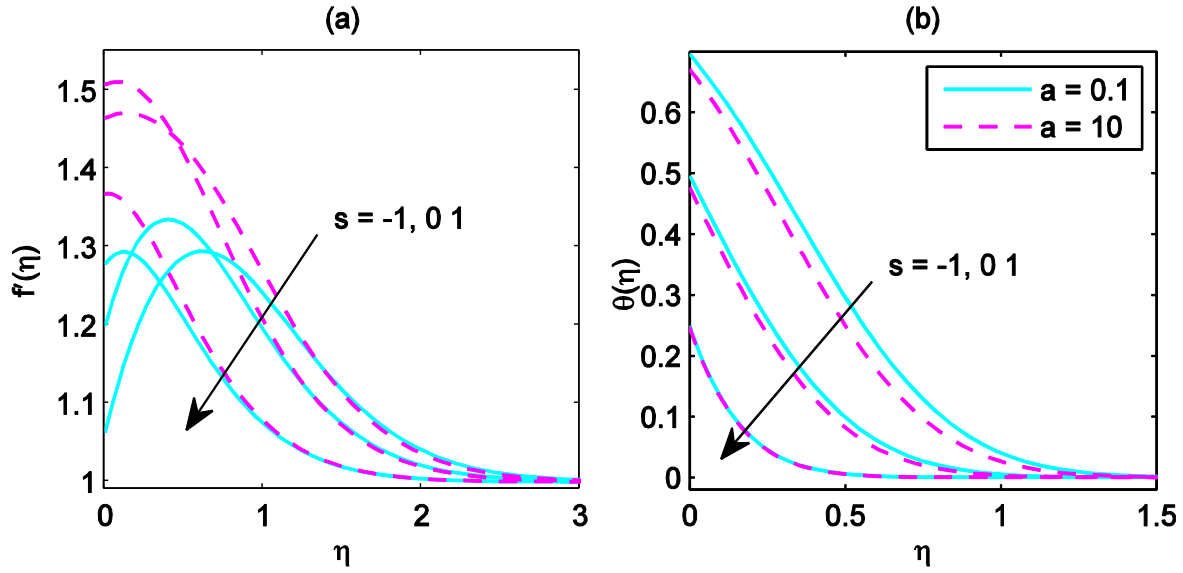

Fig. 2: Variation of $f'(\eta)$, $\theta(\eta)$ with different values of *a and s.*

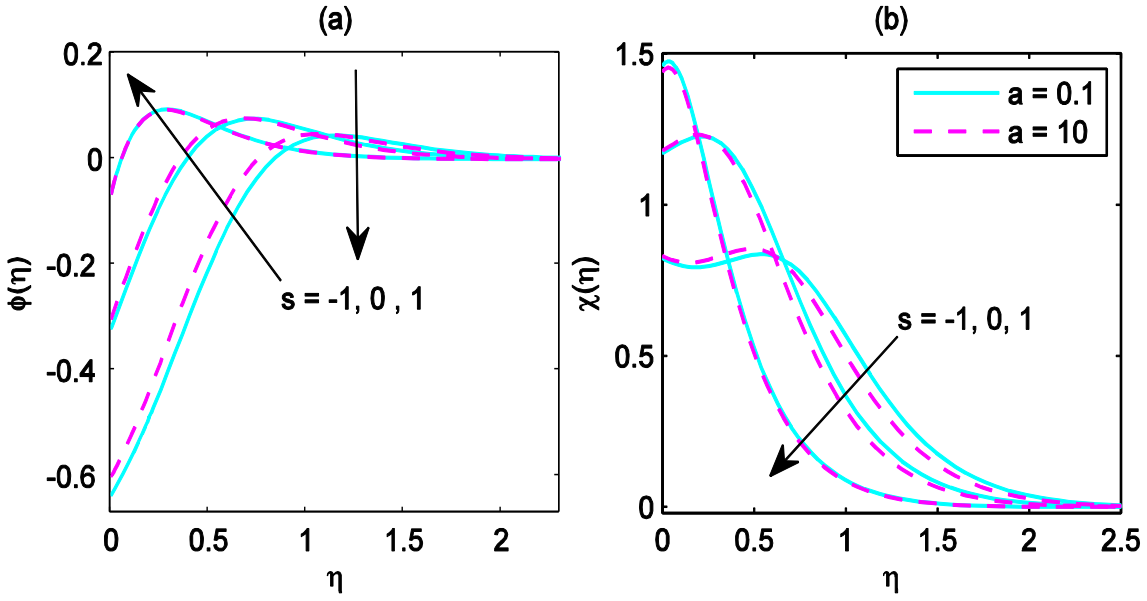

Fig. 3: Variation of $\phi(\eta)$ and $\chi(\eta)$ with different values of *a and s.*

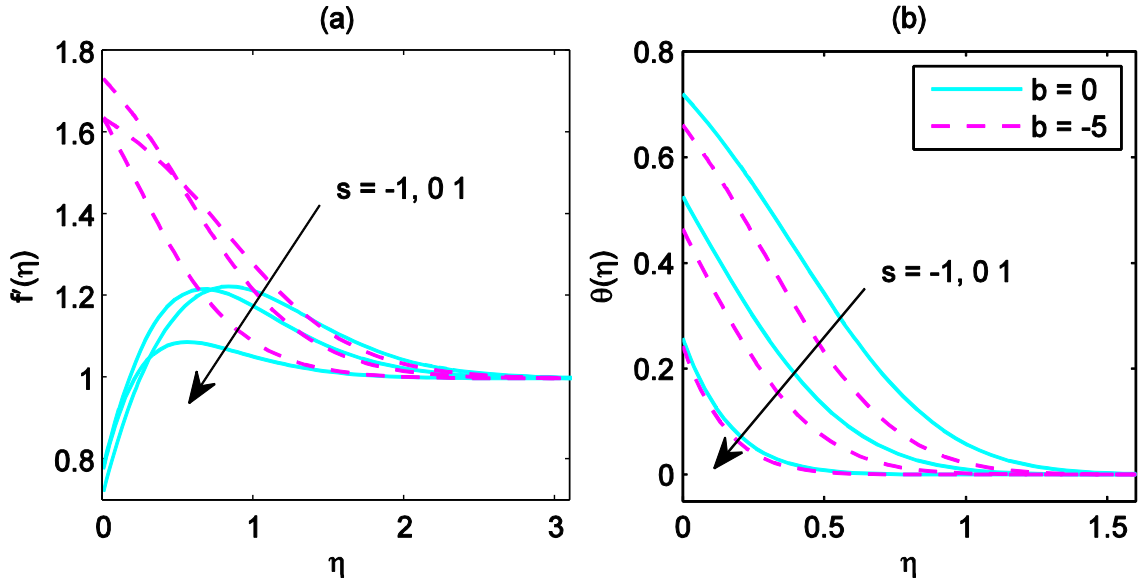

Fig.4: Variation of $f'(\eta)$ and $\theta(\eta)$ with different values of *b and s.*

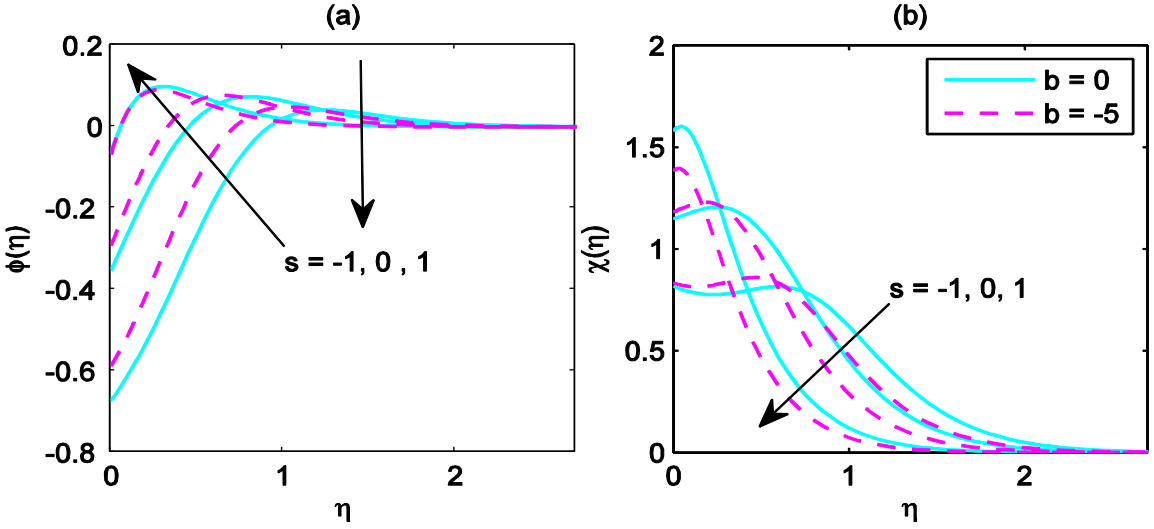

Fig. 5: Variation of $\phi(\eta)$ and $\chi(\eta)$ with different values of *b and s.*

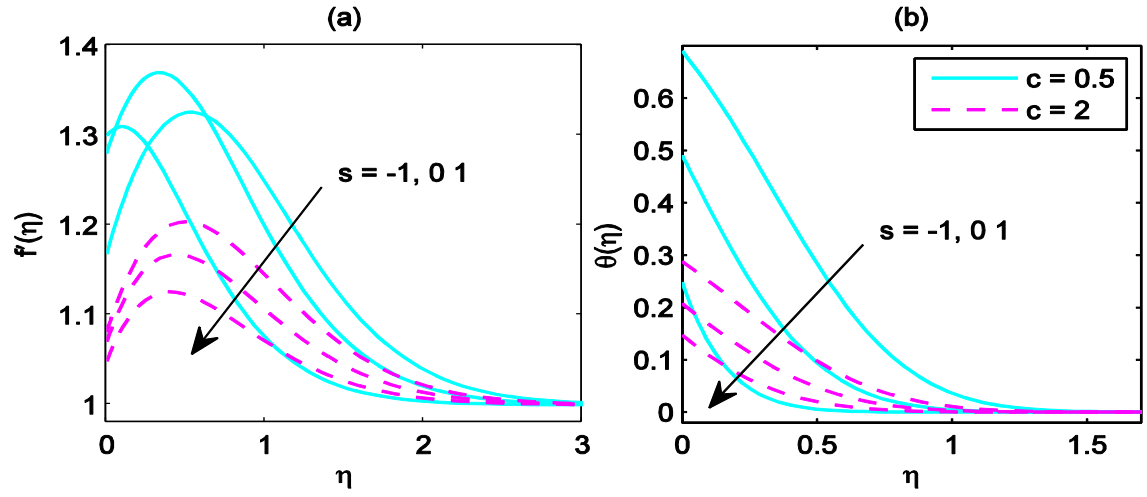

Fig.6: Variation of $f'(\eta)$ and $\theta(\eta)$ with different values of *c and s*

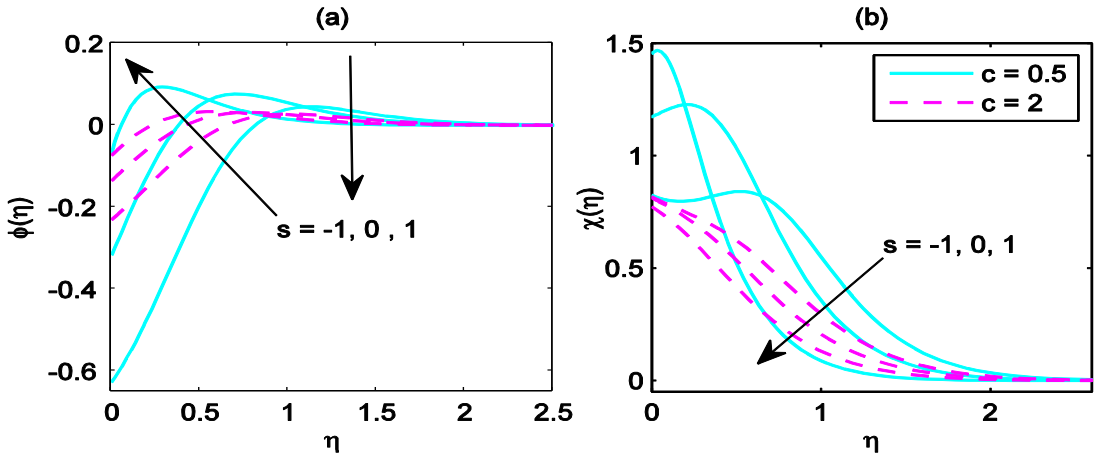

Fig. 7: Variation of $\phi(\eta)$ and $\chi(\eta)$ with different values of *c and s.*

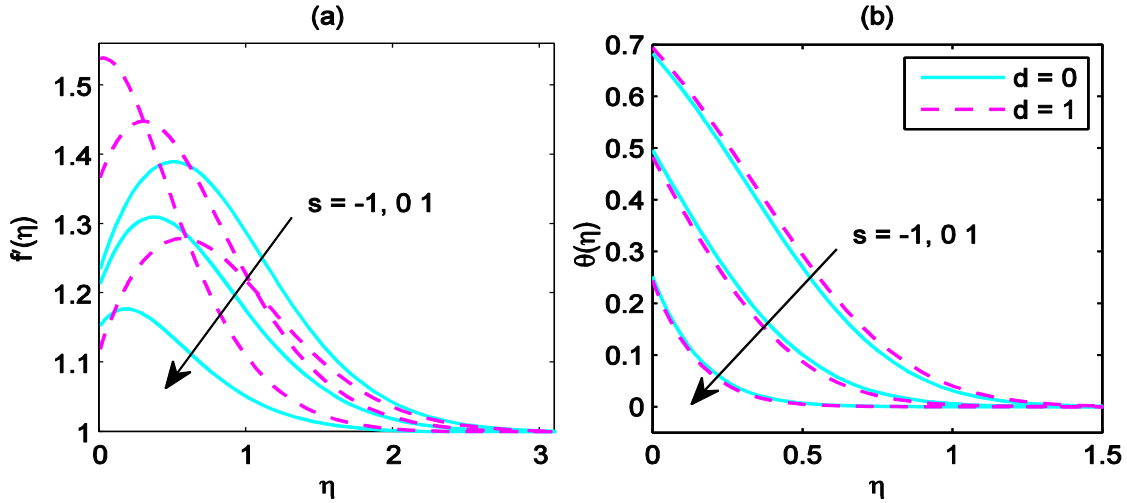

Fig.8: Variation of $f'(\eta)$ and$\theta(\eta)$ with different values of *d and s.*

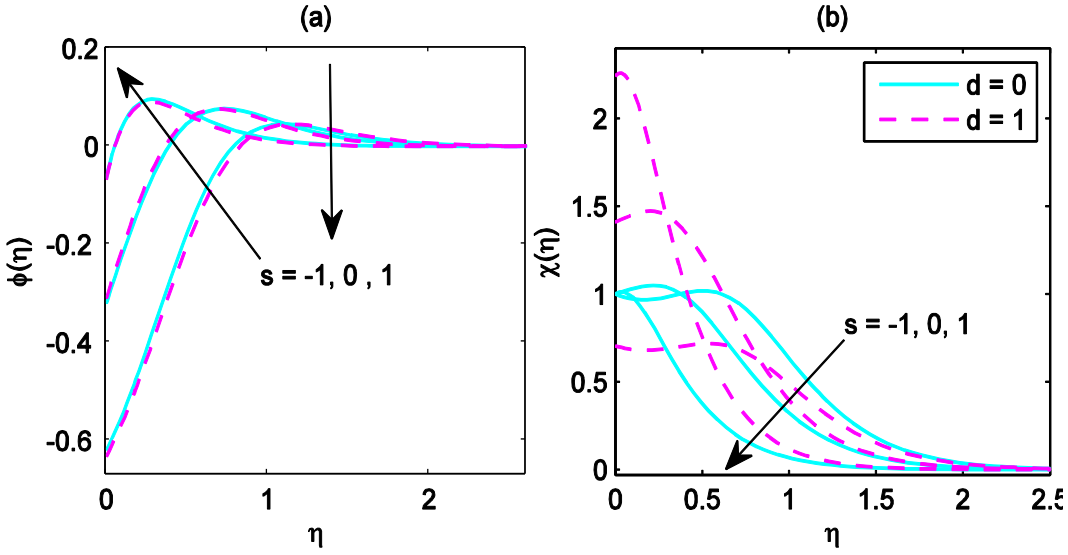

Fig. 9: Variation of $\phi(\eta)$ and $\chi(\eta)$ with different values of *d and s.*

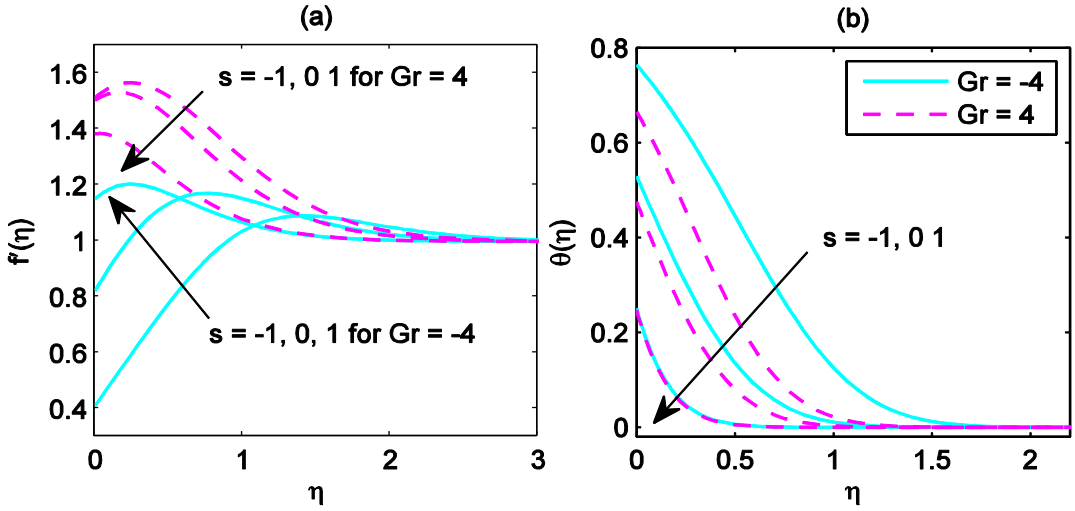

Fig.10: Variation of $f'(\eta)$ and$\theta(\eta)$ with different values of *Gr and s.*

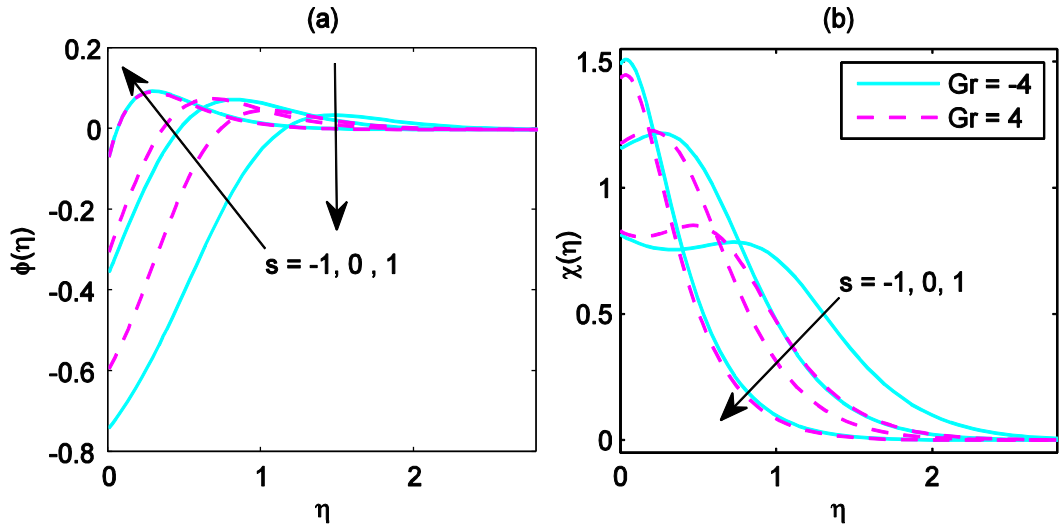

Fig. 11: Variation of $\phi(\eta)$ and $\chi(\eta)$ with different values of *Gr and s.*

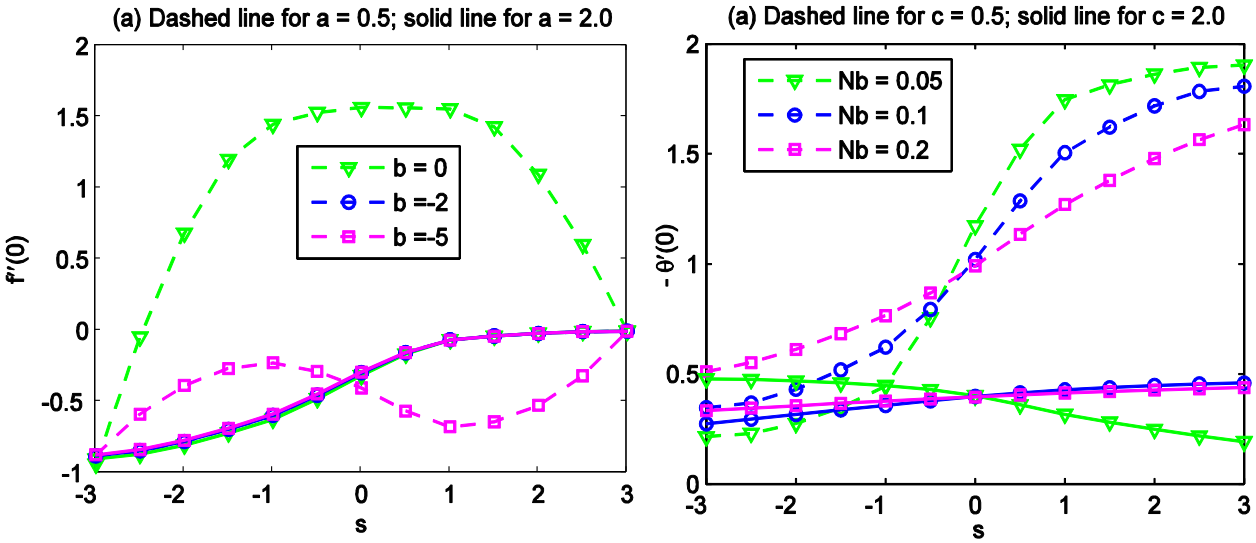

Fig.12:(a) Variation of *a* and *b* on *f*''(*0*) over *s*;(b) effect of *b* and *c* on -*θ*'(*0*)over *s.*

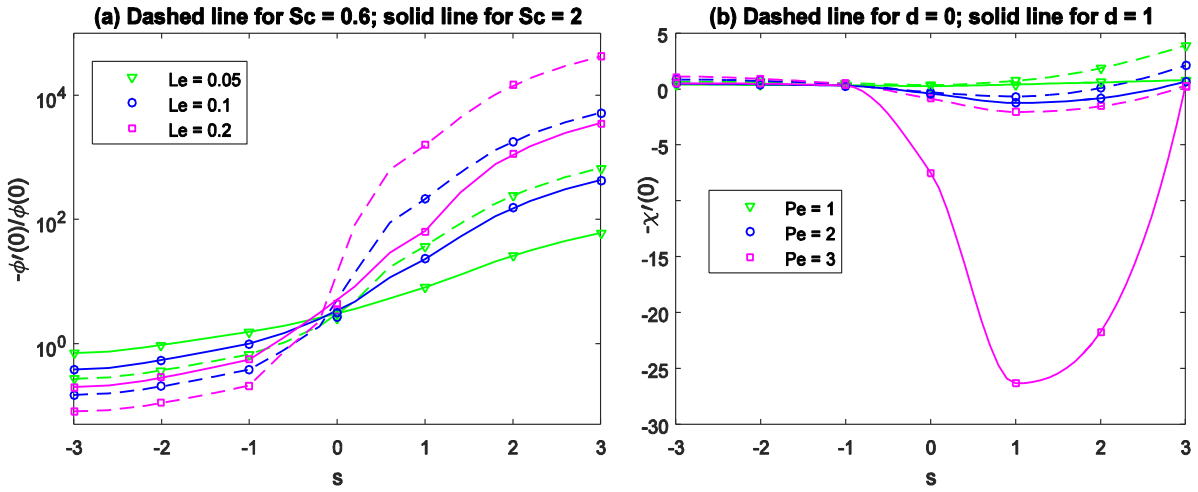

Fig. 13:(a):Effect of *Sc* and *Le* on -ϕ'(0)/ϕ (0); (b)effect of *Sc* and *Pe* on -χ′(0) over *s*.

Figs. 2(a)-(b) illustrate the collective influence of first order hydrodynamic slip (a) and wall mass flux parameter (s) on velocity and temperature distributions. With strong blowing (s=-1) the velocity is enhanced with a corresponding overshoot near the wall. This overshoot is still present with the solid wall case (s=0) but vanishes with the wall suction case (s=0). With increasing first order hydrodynamic slip, there is a significant acceleration in the flow near the wall. Temperatures are very weakly influenced by first order hydrodynamic slip and are found to be slightly reduced i.e. the regime is cooled and thermal boundary layer thickness decreases with greater first order slip. Blowing is observed to significantly elevate temperature (and thermal boundary layer thickness) whereas suction induces the opposite effect i.e. cools the regime and thermal boundary layer thickness decreases.

Figs. 3(a)-(b)present the variation in nano-particle concentration function and motile micro-organism density number function with wall mass flux and first order hydrodynamic slip. With greater suction (s>0) the nano-particle concentration increases, especially near the wall, whereas further from the wall the contrary response is computed. Blowing therefore depresses nano-particle concentration. With greater hydrodynamic slip (a), the nano-particle concentration values are weakly reduced throughout the boundary layer regime. Motile micro-organism density function conversely increases with wall suction (s>0) and enhanced with mass blowing (s<0). The effect is particularly amplified at the wall. With greater hydrodynamic slip, there is a general weak decrease in motile micro-organism density function values for both suction and solid wall cases; however there is a weak increase for the mass blowing case, close to the wall although subsequently the trend is reversed nearer the free stream.

Figs. 4(a)-(b) depict the velocity and temperature response with combined effects of wall mass flux and second order hydrodynamic slip (b). A significant deviation in profiles is observed for the velocity distributions (Fig. 4(a)) compared with those in Fig. 2(a). While second order slip substantially elevates the velocity, the profiles are all monotonic decays from the wall and there is no velocity overshoot present, as in the case of Fig 2a for first order hydrodynamic slip effects. In the absence of second order slip, the velocity profiles ascend from the wall and exhibit parabolic profiles, similar to the case when first order slip is very small (Fig. 2(a)). In all cases, irrespective of the second order slip parameter values, strong blowing (s<0) induces flow acceleration whereas strong suction generates the opposite effect. Temperatures (Fig. 4(b)) demonstrate monotonic decays and are found to be reduced with

increasing second order hydrodynamic slip effect. The effect is markedly greater than for first order hydrodynamic slip (Fig. 2(a)). Blowing is found to strongly enhance temperatures whereas suction reduces them.

Figs. 5(a)-(b) present the distributions in nano-particle concentration function and motile micro-organism density number function with wall mass flux and second order hydrodynamic slip. Very similar profiles are observed for the nano-particle concentration, for which again it is apparent that blowing reduces concentrations whereas suction enhances them. However second order slip is found to increase more prominently the concentration values than first order slip (Fig. 3(a)). Motile micro-organism density function, as plotted in Fig. 5b, is weakly elevated with blowing ($s<0$) whereas it is enhanced with wall suction ($s<0$). The effect is strongest again, close to the wall (plate). With greater second order hydrodynamic slip (b), there is consistently a reduction in motile micro-organism density function values.

Figs. 6(a)-(b) illustrate the influence of wall mass flux (s) and thermal slip on the velocity and temperature distributions. With strong blowing ($s=-1$) the velocity is significantly elevated throughout the boundary layer, and again a distinct velocity overshoot arises near the wall. With strong suction velocity magnitudes are depleted; however flow reversal is never induced as magnitudes of velocity remain positive throughout. Increasing thermal slip serves to strongly reduce velocity magnitudes i.e. decelerates the flow and increases momentum boundary layer thickness. Temperatures are also markedly depressed with greater thermal slip, c and with suction ($s>0$). Temperatures are however enhanced with blowing ($s<0$) with a corresponding increase in thermal boundary layer thickness.

Figs. 7(a)-(b) show the variation in in nano-particle concentration function and motile micro-organism density number function with wall mass flux (s) and thermal slip (c) effects. Increasing thermal slip generally decreases nano-particle concentrations especially near the wall (plate).This effect is however stifled further into the boundary layer. With greater wall suction nano-particle concentrations are effectively boosted whereas they are reduced with greater blowing effect. Increasing thermal slip is found to reduce motile micro-organism density number function values significantly and also smooths out the erratic profile for the wall blowing case. The profiles for the solid wall (plate) and wall suction are smooth monotonic decays even at low values of thermal slip. Greater suction generally decreases motile micro-organism density number function values, whereas greater injection enhances it.
Figs. 8(a)-(b) illustrate the velocity and temperature evolutions with different micro-organism (mass) slip (d) and wall mass flux (s). The flow is generally accelerated with greater mass slip effect and with greater blowing ($s<0$). Temperatures very weakly rise with greater mass slip and also with blowing, whereas they strongly fall with greater wall suction.

Figs. 9(a)-(b) show the variation in in nano-particle concentration function and motile micro-organism density number function with wall mass flux (s) and micro-organism slip (d) effects. Increasing mass slip generally results in a very slight reduction in nano-particle concentration values whereas increasing wall suction causes a strong elevation. Increasing blowing at the wall leads to significant fall in nano-particle concentrations i.e. a reduction in nano-particle concentration boundary layer thickness. Motile micro-organism density function is very strongly enhanced, in particular near the wall, with greater mass slip effect. It is also accentuated strongly with greater wall suction and markedly depleted with greater wall blowing effect.

Figs. 10(a)-(b) present the velocity and temperature field response to variation in thermal Grashof number (Gr) and wall mass flux (s) effects. With negative Gr values (implying adverse buoyancy effect), the flow is strongly decelerated whereas the converse effect is sustained for positive Gr (assistive buoyancy effect). With Gr = 4, the presence of wall blowing accelerates the flow whereas for Gr =-4 it retards the flow. The opposite effects are generated with wall suction. Temperatures are observed to be enhanced with negative Gr (opposing buoyancy) and reduced with Gr = 4 (assistive buoyancy). Wall blowing however results in rise in temperature for both negative and positive values of Grashof number, whereas wall suction results in strong drop in temperature, i.e. a *reduction in thermal boundary layer thickness*.

Figs. 11(a)-(b) show the distributions of nano-particle concentration function and motile micro-organism density number function with a change in thermal Grashof number (Gr) and wall mass flux (s). Negative Gr values (opposing buoyancy) generally induce a reduction in nano-particle concentrations whereas positive Gr values generate the contrary effect. This is especially prevalent for the solid wall and blowing cases. With increasing suction nano-particle concentrations are boosted whereas they are lowered with greater blowing at the wall. Motile micro-organism density function is found to be generally reduced with positive Gr values whereas it is higher for negative Gr values. Micro-organism density is therefore encouraged with opposing buoyancy and inhibited with assistive buoyancy. Increasing wall suction tends to reduce significantly values of micro-organism density function throughout the boundary layer regime, whereas wall blowing generates the converse trend.

Fig.12(a) illustrates the collective effects of first (a) and second order hydrodynamic slip (b) and wall mass flux (s) parameters on wall skin friction (surface shear stress function) Increasing first order slip massively reduces skin friction for any value of *s*. Increasing second order hydrodynamic slip also generally reduces the wall skin friction. However greater values are computed when wall suction is present (s>0) compared to when wall blowing is present (s<0).

Fig. 12(b)shows the response in wall heat transfer rate (temperature gradient) with different values of thermal slip (c), Brownian motion parameter (Nb) and wall mass flux parameter (s). Increasing thermal slip generally strongly reduces the wall heat transfer rate when wall suction is present; however when wall blowing is present there is a slight decrease in heat transfer rates. With increasing Brownian motion effect (higher Nb values), the nano-particles are reduced in size. This decreases the heat transfer rate to the wall since greater temperatures are induced in the body of the fluid with smaller nano-particles and thermal energy is retained in the fluid with lower transport rates to the wall. The opposite effect is apparent with smaller Nb values which imply larger nano-particles, lower temperatures and therefore higher heat transfer rates to the wall.

Finally,**Figs. 13(a)-(b)** demonstrate the effects of different bioconvection parameters (bioconvection Schmidt number, Lewis number and Péclet number) on the nano-particle wall mass transfer rate and the motile micro-organism wall mass transfer rate, respectively. In Fig. 13(a), increasing bioconvection Lewis number (Le) significantly reduces the nano-particle wall mass transfer rate when blowing is present (s<0) whereas it enhances it when suction is present (s>0). With increasing Schmidt number (*Sc*) nano-particle wall mass transfer rate is elevated for the case of wall injection (s<0) whereas for wall suction (s>0) the opposite effect is induced. In Fig. 13(b), with greater bioconvection Péclet number, there is a strong depletion in the motile micro-organism wall mass transfer rate when suction is present. However when

injection (mass lowing) is present, there is a very weak increase in motile micro-organism wall mass transfer rate. Increasing micro-organism wall mass slip parameter (d) is found to slightly reduce motile micro-organism wall mass transfer rate when wall injection (s<0) is present but induces a massive decrease when wall suction (s>0) is present.

8. CONCLUSIONS

A mathematical model has been developed for 2-dimensional, steady laminar incompressible gyrotactic bioconvection boundary layer flow of a nanofluid from an upward facing horizontal permeable plate adjacent to a porous medium. First and second order hydrodynamic slip, thermal slip and also microorganism mass slip at the wall have been incorporated, as have passive nanofluid boundary conditions at the wall (plate). Wall mass (Stefan blowing or suction) effects have also been studied as these are significant also in nano-bio-materials processing. The transformed similarity ordinary differential equations have been derived using Lie group analysis. The resulting, well-posed ordinary differential two-point boundary value problem has been solved with Chebyshev collocation algorithm. Verification of the numerical solutions has been achieved with an alternative computational technique, namely the Nakamura tridiagonal second order finite difference method. Very good correlation has been achieved with extensive details of both methods described. Additionally, validation with previous published solutions has also been included. A parametric investigation of the influence of the emerging bioconvection, nanofluid and other thermophysical parameters on the evolution of velocity, skin friction, temperature, heat transfer rate, nano-particle concentration, nano-particle wall mass transfer rate, motile micro-organism density number function and wall micro-organism mass transfer rate has been conducted. Some key observations from the present computations are:

(i)There is greater sensitivity of the velocity field to second order slip then first order hydrodynamic slip.

(ii)Thermal and mass slip also exert a strong effect on nano-particle and micro-organism density distributions.

(iii) Wall suction induces significant deceleration effects in the velocity field whereas it is observed to enhance nano-particle and motile micro-organism concentrations.

(iv)Mass slip is found to increase micro-organism density function, temperature and velocity whereas it reduces slightly the nano-particle concentration.

(v)Positive Grashof number is observed to accelerate the bioconvection nanofluid boundary layer flow and also raise temperatures and nano-particle concentrations, whereas it reduces the motile micro-organism density function.

The effects of other parameters including Brownian motion, bioconvection Lewis number, Schmidt number and Péclet number on the transport variables are also elucidated in detail. The present model has been confined to *steady-state Newtonian* flow. Future investigations will address both *time-dependent and non-Newtonian* bioconvection nanofluid flows in porous media, and these are also relevant to nano-materials processing operations.

SYMBOLS USED

b chemotaxis constant

$\overline{C}$ nanoparticle volume fraction

$\overline{C}_w$ wall nanoparticle volume fraction

$\overline{C}_\infty$ ambient nanoparticle volume fraction

D_B Brownian diffusion coefficient

D_n diffusivity of microorganisms

D_T thermophoretic diffusion coefficient
$f(\eta)$ dimensionless stream function
g acceleration due to gravity
$\bar{\mathbf{j}}$ vector flux of microorganism
k thermal conductivity
K consistency coefficient
K_0 permeability of the porous medium
L characteristic length
Lb bioconvection Lewis number
Le Lewis number
m power law index
$\bar{n}_n$ volume fraction of motile microorganisms
Nb Brownian motion parameter
$Nn_{\bar{x}}$ local density number of the motile microorganisms
Nt thermophoresis parameter
$Nu_{\bar{x}}$ localNusselt number
Pe bioconvection Péclet number
Pr Prandtl number
$\bar{p}$ pressure
$\bar{q}_m$ wall mass flux
$\bar{q}_n$ wall motile microorganisms flux
$\bar{q}_w$ wall heat flux
Ra Rayleigh number for the porous medium
$Ra_{\bar{x}}$ local Rayleigh number for the porous medium
Rb bioconvection Rayleigh number
$Sh_{\bar{x}}$ local Sherwood number
$\bar{T}$ nanofluid temperature
$\bar{T}_w$ wall temperature
$\bar{T}_\infty$ ambient temperature
$\bar{u}, \bar{v}$ velocity components along $\bar{x}-$ and $\bar{y}-$axes
$\tilde{\bar{u}}, \tilde{\bar{v}}$ average directional swimming velocity of microorganisms along axes
W_c constant maximum cell swimming speed
$\bar{x}, \bar{y}$ Cartesian coordinates ($\bar{x}-$axis is aligned along and $\bar{y}-$axis is normal to the plate)

Greek symbols

α_m effective thermal diffusivity of the porous medium
$\phi(\eta)$ rescaled nanoparticle volume fraction
η similarity variable
γ density of motile microorganisms
$\theta(\eta)$ dimensionless temperature
ν kinematic viscosity of the fluid
ρ_f fluid density

ρ_p nanoparticle mass density
$(\rho c)_f$ heat capacity of the fluid
$(\rho c)_p$ heat capacity of the nanoparticle material
τ ratio between effective heat capacity of nanoparticles and heat capacity of fluid
$\sigma(\eta)$ rescaled density of motile microorganisms
ψ stream function

Subscripts/superscripts
w condition at the wall
∞ free stream condition
' differentiation with respect to η

REFERENCES

Bég, O. Anwar, Numerical methods for multi-physical magnetohydrodynamics, Chapter1, pp. 1-112, *New Developments in Hydrodynamics Research, M. J. Ibragimov and M. A. Anisimov, Eds*., *Nova Science, New York, September* (2012).

Bég, O. Anwar, NANONAK- A finite difference code for nanofluid convection problems of the boundary layer type, *Technical Report, NANO-C/5-1, 124pp, Gort Engovation-Aerospace and Ocean Engineering Sciences, Bradford, England/Narvik, Norway, UK, August* (2013).

Bég, O. Anwar, T. A. Bég, H. S. Takhar, A. Raptis, Mathematical and numerical modeling of non-Newtonian thermo-hydrodynamic flow in non-Darcy porous media, *Int. J. Fluid Mech. Res.*, 31, 1–12 (2004).

Bég, O. Anwar, J. Zueco, M. Norouzi, M. Davoodi, A. A. Joneidi, Assma F. Elsayed, Network and Nakamura tridiagonal computational simulation of electrically-conducting biopolymer micro-morphic transport phenomena, *Computers in Biology and Medicine*, 44, 44–56 (2014).

Bég, O. Anwar, V.R. Prasad, B. Vasu, Numerical study of mixed bioconvection in porous media saturated with nanofluid and containing oxytactic micro-organisms, *J. Mechanics Medicine Biology*, 13, 1350067.1-1350067.25 (2013).

Bég, O. Anwar, Md. Jashim Uddin and W.A. Khan, Bioconvective non-Newtonian nanofluid transport in porous media containing micro-organisms in a moving free stream, *J. Mechanics Medicine Biology*, 15, 1550071.1-1550071.20 (2015).

Beskok, A. and Karniadakis, G.E., Simulation of heat and momentum transfer in complex micro-geometries, *AIAA J. Thermophysics Heat Transfer*, 8, 355-370 (1994).

Buongiorno, J., Convective transport in nanofluids, *ASME J. Heat Transfer*,128, 240–250, (2006).

Cantwell, B. J., *Introduction to Symmetry Analysis*, Cambridge University Press (2002).

Das, K., Slip flow and convective heat transfer of nanofluids over a permeable stretching surface, *Computers & Fluids*, 64, 34–42 (2012).

Das, K., P. R. Duari, P.K. Kundu, Nanofluid bioconvection in presence of gyrotactic microorganisms and chemical reaction in a porous medium, *J. Mech. Sci. Tech.*, 29, 4841-4849 (2015).

Fang, T. *et al*. (2010),Viscous flow over a shrinking sheet with a second order slip flow model, *Commun. in Nonl. Sci. and Numer. Simul*. 15, 1831-1842.

Fang, T. and Abdul Aziz (2010),Viscous flow with second-order slip velocity over a stretching sheet, *Zeitschrift für Naturforschung, A* 65,1087-1092.

Fang, T. (2014). Flow and mass transfer for an unsteady stagnation-point flow over a moving wall considering blowing effects, *ASME J. Fluids Engineering*,136(7), 071103

Fang, T., & Jing, W., Flow, heat, and species transfer over a stretching plate considering coupled Stefan blowing effects from species transfer, *Comm. Nonlinear Science and Numerical Simulation*, 19(9), 3086-3097 (2014).

Gebhart, B. et al, *Buoyancy-induced Flows and Transport*, Hemisphere, Washington (1988).

Gorla, R.S.R. and S. Nakamura, Combined convection from a rotating cone to micropolar fluids, *Math. Modelling Sci.Comput*., 2, 1249–1254 (1993).

Iliuta, I., B.P.A. Grandjean, F. Larach Hydrodynamics of trickle-flow reactors: updated slip functions for the slit models, *Chemical Engineering Research and Design*, 80, 195-200 (2002).

Karniadakis, G.E. *et al*., *Microflows and Nanoflows: Fundamentals and Simulation*, Springer, New York (2005).

Kothandapani, M. and J. Prakash, Effects of thermal radiation and chemical reactions on peristaltic flow of a Newtonian nanofluid under inclined magnetic field in a generalized vertical channel using homotopy perturbation method, *Asia-Pacific J. Chemical Engineering*, 10, 259–272 (2015).

Kuznetsov, A.V., The onset of nanofluid bioconvection in a suspension containing both nanoparticles and gyrotactic microorganisms. *Int. Comm. Heat Mass Transfer*, 37 (2010) 1421-1425.

Kuznetsov, A. V. Nanofluid bio-thermal convection: simultaneous effects of gyrotactic and oxytactic micro-organisms, *Fluid Dynamics Research* 43.5 (2011a): 055505.

Kuznetsov, A.V. Non-oscillatory and oscillatory nanofluid bio-thermal convection in a horizontal layer of finite depth,*Euro. J. Mech.-B/Fluids*, 30 (2011b) 156-165.

Kuznetsov, A.V., Nanofluid bioconvection in water-based suspensions containing nanoparticles and oxytactic microorganisms: oscillatory instability. *Nanoscale Res. Letters*, (2011c):6, 100.

Kuznetsov, A. V., and D. A. Nield., The Cheng–Minkowycz problem for natural convective boundary layer flow in a porous medium saturated by a nanofluid: a revised model, *International Journal of Heat and Mass Transfer* 65 (2013): 682-685.

Kuznetsov, A.V., D.A. Nield, Natural convective boundary-layer flow of a nanofluid past a vertical plate: A revised model, *International Journal of Thermal Sciences,* 77 (2014) 126-129.

Lawal, D. and M. Kalyon, Viscous heating in non-isothermal die flows of viscoplastic fluids with wall slip, *Chemical Engineering Science*, 52, 1323-1337 (1997).

Mustafa, M. and J.A. Khan, Model for flow of Casson nanofluid past a non-linearly stretching sheet considering magnetic field effects, *AIP Advances* 5, 077148 (2015).

Nakamura, S., Iterative finite difference schemes for similar and non-similar boundary layer equations, *Adv. Eng. Software*, 21, 123–130 (1994).

Nakamura, S., *Applied Numerical Methods and Software*, Prentice-Hall New Jersey, USA (1995).

Nield, D. A., and A. V. Kuznetsov.The Cheng–Minkowycz problem for natural convective boundary-layer flow in a porous medium saturated by a nanofluid, *International Journal of Heat and Mass Transfer* 52.25 (2009): 5792-5795.

Platt, J.R., Bioconvection patterns in cultures of free swimming organisms, *Science*, 133:1766-1767 (1961).

Prasad, V.R., S. A. Gaffar and O. Anwar Bég, Heat and mass transfer of a nanofluid from a horizontal cylinder to a micropolar fluid, *AIAA J. Thermophysics Heat Transfer*, 29, 1, 127-139 (2015).

Rana, P. and O. Anwar Bég, Mixed convection flow along an inclined permeable plate: effect of magnetic field, nanolayer conductivity and nanoparticle diameter, *Applied Nanoscience* (2014). 13 pages. DOI 10.1007/s13204-014-0352-z

Tham, L., R. Nazar, and I. Pop. Steady mixed convection flow on a horizontal circular cylinder embedded in a porous medium filled by a nanofluid containing gyrotactic micro-organisms, *ASME Journal of Heat Transfer*, 135.10 (2013a): 102601.

Tham, L., R.Nazar, and I. Pop. Mixed convection flow over a solid sphere embedded in a porous medium filled by a nanofluid containing gyrotactic microorganisms. *International Journal of Heat and Mass Transfer* 62 (2013b): 647-660.

Tiwari, R.K. and Das, M.K. Heat transfer augmentation in a two-sided lid-driven differentially heated square cavity utilizing nanofluids, *Int. J. Heat Mass Transfer*, 50, 2002–2018 (2007).

Uddin, M.J., O. Anwar Bég and N. Amin, Hydromagnetic transport phenomena from a stretching or shrinking nonlinear nanomaterial sheet with Navier slip and convective heating: A model for bio-nano-materials processing, *J. Magnetism and Magnetic Materials*, 368, 252-261 (2014).

Uddin, M.J., O. Anwar Bég, A. Aziz and A. I. M. Ismail, Group analysis of free convection flow of a magnetic nanofluid with chemical reaction, *Math. Prob. Engineering*, 2015, Article ID 621503, 11 pp (2015). doi:10.1155/2015/621503.

Uddin,M.J., Kabir, M.N., Y. Alginahi, Lie group analysis and numerical solution of magnetohydrodynamic free convective slip flow of micropolar fluid over a moving plate with heat transfer, *Computers & Mathematics with Applications* 70(5), 846-856(2015a).

Wu , L. (2008), A slip model for rarefied gas flows at arbitrary Knudsen number, *Appl. Phy. Lett*, 93, 253103

Xu, H., Lie Group analysis of a nanofluid bioconvection flow past a vertical flat surface with an outer power-law stream, *ASME J. Heat Transfer*, 137(4), 041101 (2015).

Xu, H. and I. Pop. Fully developed mixed convection flow in a horizontal channel filled by a nanofluid containing both nanoparticles and gyrotactic microorganisms. *European J. Mechanics-B/Fluids* 46 (2014): 37-45.

Yadav, D., R. Bhargava, G. S. Agrawal, G. S. Hwang, J. Lee and M. C. Kim, Magneto-convection in a rotating layer of nanofluid, *Asia-Pacific J. Chemical Engineering*, 9, 663–677 (2014).

Zaimi, K. A. Ishak and I. Pop, Stagnation-point flow toward a stretching/shrinking sheet in a nanofluid containing both nanoparticles and gyrotactic microorganisms, *ASME J. Heat Transfer*, 136(4), 041705 (2014a).

Zaimi, K., A. Ishak, I. Pop, Unsteady flow due to a contracting cylinder in a nanofluid using Buongiorno's model. *Int. J. Heat Mass Transfer*, 68 (2014b) 509-513.